
Charge Qubit Coupled to Quantum Telegraph Noise

Florian Schröder



München 2012

Charge Qubit Coupled to Quantum Telegraph Noise

Florian Schröder

Bachelorarbeit
an der Fakultät für Physik
der Ludwig-Maximilians-Universität
München

vorgelegt von
Florian Schröder
aus München

München, den 20. Juli 2012

Gutachter: Prof. Dr. Jan von Delft

Contents

Abstract	vii
1 Introduction	1
1.1 Time Evolution of Closed Quantum Systems	2
1.1.1 Schrödinger Picture	2
1.1.2 Heisenberg Picture	3
1.1.3 Interaction Picture	3
1.2 Description of the System of Qubit and Bath	4
2 Quantum Telegraph Noise Model	7
2.1 Hamiltonian	7
2.2 The Master Equation	7
2.3 DMRG and Model Parameters	11
2.3.1 D, Δ, γ and ϵ_d	11
2.3.2 Discretization and Bath Length	11
3 The Periodically Driven Qubit	15
3.1 The Full Model	15
3.2 Rabi Oscillations	15
3.2.1 Pulses	17
3.3 Bloch-Siegert Shift	18
3.3.1 Finding the Bloch-Siegert Shift	18
3.4 Driven Qubit Coupled to QTN	21
3.5 Simulations of Spin Echo and Bang-Bang with Ideal π -Pulses	23
4 Conclusion and Outlook	27
A Derivations	29
A.1 Master Equation	29
A.1.1 Projection Operator Method	29
A.1.2 Interaction Picture Hamiltonian	31
A.1.3 Bath Correlation Functions	33
A.2 Discrete Fourier Transformation	36

A.3	Solution of the Rabi Problem	39
A.3.1	Rotating-Wave-Approximation	39
A.3.2	Bloch-Siegert Shift	40
A.4	Jaynes-Cummings-Hamiltonian	41
	Bibliography	47
	Acknowledgements	48

Abstract

I simulate the time evolution of a qubit which is exposed to quantum telegraph noise (QTN) with the time-dependent density matrix renormalization group (t-DMRG). After studying the decoherence of the qubit, we simulate pulse manipulations on the qubit with the aim of reducing its overall rate of decoherence. The main part of this work presents the related topics of Rabi oscillations and the Bloch-Siegert shift which are important to derive the conditions under which such operations are possible.

First the interaction between the qubit and the QTN is studied analytically by deriving a quantum master equation (QME) in the Born-Markov approximation. Then based on the exact results of Ref.[2] for the qubit decoherence, the t-DMRG simulation is calibrated.

Afterwards we extend the QTN model by adding an external periodical driving field which is intended to perform pulse protocols like spin echo and bang-bang. To properly understand the interaction between the qubit and the driving field, we present Rabi oscillations. Additionally for strong driving fields, the Bloch-Siegert shift combined with a method of measurement is studied. Then Rabi oscillations are simulated with t-DMRG under different couplings to the QTN to derive conditions needed for properly working π -pulses. In the end the spin echo and bang-bang protocol, performed with ideal π -Pulses are simulated to study their efficiency in maintaining coherence of a qubit exposed to QTN.

Chapter 1

Introduction

Quantum two-level systems are very important for quantum physics as they can be used for modelling parts of multi-level systems, for example atoms or quantum dots [38]. Under the name of Qubits, they are the main ingredient for quantum computation which opens a door to a whole range of new possibilities for information processing. Besides the application of classical bit operations, qubits allow quantum gate operations, which for instance can modify the phase and entanglement of qubits [11]. However a very serious problem is the rapid decoherence of the qubit which is caused by the inevitable interaction with its environment. The decoherence is equivalent to a loss of information making the qubit useless for computations. Typical coherence times (T_2) during which it is possible to perform quantum gate operations on qubits are currently in the order of μs as in Josephson junction qubits [23]. But for computations consisting of quantum algorithms and quantum error correction, the coherence time should be much longer than $10^5 \tau_g$ the minimum gate operation time which is determined by the qubit's energy level spacing [20]. A very promising approach to conserve coherence is called dynamical decoupling which basically aims to decouple the system of interest from its environment by applying a certain sequence of controlling pulses. In the last decade several protocols have been proposed, for example bang-bang control [35, 34], Carr-Purcell-Meiboom-Gill sequence [10, 19], concatenated dynamical decoupling [17] and Uhrig dynamical decoupling [32] [37].

The density matrix renormalization group (DMRG) was invented in 1992 by S. White and is a very accurate and efficient numerical method to calculate ground states of one-dimensional quantum lattices. With the adaptive time-dependent DMRG (t-DMRG) it is possible to simulate the dynamics of those systems. We use t-DMRG to simulate the whole interacting quantum system consisting of a qubit and the environment which is chosen here to be a quantum telegraph noise model (QTNM) [1]. The QTNM consists of a non-interacting electron reservoir which is tunnel coupled to an impurity. This impurity is spin-polarized such that only one electron can occupy it. The fluctuation of charge on the impurity creates the quantum telegraph noise (QTN) acting on the qubit. The t-DMRG simulation of this system including an external periodical driving field enables to observe the influence of QTN on the accuracy of pulses in general and the efficiency of noise cancelling pulse protocols in particular. This thesis will do preparatory work and analytical

approaches for those simulations.

In the first part we give an analytical solution for the case of a weak coupling between the qubit and the QTN. Afterwards a strong interaction will be simulated with t-DMRG to compare results with analytical work done in Ref.[2] and to calibrate the simulation for further computations.

The second part will be concerned with the effect of an external periodical driving field thus presenting Rabi oscillations. We study additionally the Bloch-Siegert shift as this becomes important for strong pulses. Subsequently t-DMRG will be used to study the effect of the spin echo and bang-bang protocol under QTN for ideal π -pulses. These ideal pulses are not generated by the driving field but artificially applied to the qubit state, to enable a separate observation of pulse and protocol errors.

This thesis will generally follow notations and conventions used in Ref.[6, 7, 28]. But for convenience this chapter shall give the most important properties in a short overview.

1.1 Time Evolution of Closed Quantum Systems

1.1.1 Schrödinger Picture

For a time-dependent Hamiltonian of a closed system, the time evolution of an initial state $|\Psi_0\rangle$ is determined by the Schrödinger equation

$$\begin{aligned} i\frac{d}{dt}|\Psi(t)\rangle &= H(t)|\Psi(t)\rangle \\ |\Psi(t)\rangle &= U(t, t_0)|\Psi_0\rangle = \mathcal{T}e^{-i\int_{t_0}^t H(t')dt'}|\Psi_0\rangle. \end{aligned} \quad (1.1)$$

Here the convention $\hbar = 1$ is used which is convenient as it simplifies calculations and implies that energy and angular frequency have the same units. If the Hamiltonian is time-independent, the unitary time-evolution operator $U(t, t_0)$ simplifies to

$$U(t, t_0) = e^{-iH(t-t_0)}|\Psi_0\rangle. \quad (1.2)$$

In analogy the time evolution of the density matrix

$$\begin{aligned} \rho_0 &= \sum_i w_i |\Psi_i(t_0)\rangle \langle \Psi_i(t_0)| \\ \rho(t) &= \sum_i w_i |\Psi_i(t)\rangle \langle \Psi_i(t)| = U(t, t_0)\rho_0 U^\dagger(t, t_0) \end{aligned} \quad (1.3)$$

can be expressed as

$$\frac{d}{dt}\rho(t) = -i[H(t), \rho(t)], \quad (1.4)$$

which is called the Liouville-von Neumann equation.

1.1.2 Heisenberg Picture

In the Heisenberg picture the time dependence is moved from the states to the operators. Thus

$$\begin{aligned} |\Psi_H\rangle &= |\Psi_0\rangle, \\ \rho_H &= \rho_0, \\ A_H(t) &= U^\dagger(t, t_0)A(t_0)U(t, t_0), \\ \Rightarrow \frac{d}{dt}A_H(t) &= i[H, A_H(t)] + \frac{\partial}{\partial t}A_H(t), \end{aligned} \tag{1.5}$$

with the same definition of the time-evolution operator $U(t, t_0)$ as in the Schrödinger picture.

1.1.3 Interaction Picture

For a Hamiltonian with an interaction term $H_I(t)$ of the form

$$H(t) = H_0 + H_I(t), \tag{1.6}$$

a change from the Schrödinger to the interaction picture can be made to separate time dependence of H_0 from the states to the operators. The interaction picture states $|\Psi_I(t)\rangle$ and operators $\tilde{A}(t)$ can be derived from the Schrödinger picture quantities $|\Psi(t)\rangle$ and A

$$|\Psi_I(t)\rangle = U_0^\dagger(t, t_0) |\Psi(t)\rangle, \tag{1.7}$$

$$\tilde{A}(t) = U_0^\dagger(t, t_0) A U_0(t, t_0), \tag{1.8}$$

$$U_0(t, t_0) = e^{-iH_0(t-t_0)}. \tag{1.9}$$

Thus the Schrödinger equation and its solution modifies to

$$i \frac{d}{dt} |\Psi_I(t)\rangle = H_I(t) |\Psi_I(t)\rangle, \tag{1.10}$$

$$|\Psi_I(t)\rangle = U_I(t, t_0) |\Psi_I(t_0)\rangle = \mathcal{T} e^{-i \int_{t_0}^t H_I(t') dt'} |\Psi_I(t_0)\rangle. \tag{1.11}$$

For the interaction picture density matrix $\tilde{\rho}(t)$ following relations can be derived

$$\tilde{\rho}(t) = U_0^\dagger(t, t_0) \rho(t) U_0(t, t_0) = U_I(t, t_0) \rho(t_0) U_I^\dagger(t, t_0), \tag{1.12}$$

$$\frac{d}{dt} \tilde{\rho}(t) = -i[\tilde{H}_I(t), \tilde{\rho}(t)], \tag{1.13}$$

$$\frac{d}{dt} \rho(t) = -i[H_0, \rho(t)] + U_0(t, t_0) \left(\frac{d}{dt} \tilde{\rho}(t) \right) U_0^\dagger(t, t_0). \tag{1.14}$$

1.2 Description of the System of Qubit and Bath

The main part of this thesis will concentrate on the time evolution of one example of dissipative quantum impurity systems: a qubit embedded in a noisy environment. We will use a quantum master equation to study time evolution of the system. For a Hamiltonian describing the whole model of qubit and an external bath

$$H(t) = H_S + H_B + H_I(t), \quad (1.15)$$

the states of its Hilbert space are generally a combination of system eigenstates $|s_i\rangle$ and bath states $|B_i\rangle$

$$|\Psi\rangle = \sum_i c_i |s_i\rangle |B_i\rangle, \quad (1.16)$$

with $|B_i\rangle = \sum_l a_{l,i} |b_l\rangle$ being a superposition of bath eigenstates. From the density matrix $\rho(t) = |\Psi(t)\rangle\langle\Psi(t)|$ of the whole system, the reduced density matrix of the qubit ρ_S can be calculated with the partial trace over bath states

$$\rho_S = \text{tr}_B\{\rho\} = \sum_l \langle b_l | \rho | b_l \rangle, \quad (1.17)$$

which leads to its time evolution

$$\begin{aligned} \rho_S(t) &= \text{tr}_B\{\rho(t)\}, \\ \frac{d}{dt}\rho_S(t) &= -i\text{tr}_B\{[H(t), \rho(t)]\}. \end{aligned} \quad (1.18)$$

Furthermore the trace over an observable O with the density ρ_B of a thermal equilibrium state of the bath is the thermal expectation value

$$\text{tr}_B\{O\rho_B\} = \langle O \rangle_{\rho_B}. \quad (1.19)$$

The coherence of the qubit can be measured by the visibility D

$$|D(t)| = 2 |\rho_{S,\uparrow\downarrow}(t)|, \quad (1.20)$$

where $\rho_{S,\uparrow\downarrow}(t)$ is the off-diagonal entry of the hermitian reduced density matrix ρ_S . This means that for vanishing off-diagonal entries visibility and coherence decreases, which also means that the qubit is in a mixed state.

In combination with the bloch vector representation the visibility can be also depicted in another way. With the general definition of a bloch vector $\vec{a} = (a_x, a_y, a_z)$ for an arbitrary 2-dimensional density matrix ρ

$$\rho = \frac{1}{2} \begin{pmatrix} 1 + a_z & (a_x - ia_y) e^{i\delta t} \\ (a_x + ia_y) e^{-i\delta t} & 1 - a_z \end{pmatrix}, \quad (1.21)$$

the visibility becomes

$$|D(t)| = 2 |\rho_{S,\uparrow\downarrow}(t)| = 2 \cdot \frac{1}{2} \sqrt{a_x^2 + a_y^2}, \quad (1.22)$$

which is the length of the bloch vector projected onto the $x - y$ plane. In this definition the factor $e^{\pm i\delta t}$ is included as it is sometimes used in the literature to change to an external rotating frame, however it does not influence the relation for the visibility.

Chapter 2

Quantum Telegraph Noise Model

2.1 Hamiltonian

The model used to calibrate the t-DMRG implementation is a charge qubit coupled to a quantum telegraph noise (QTN) which is discussed in Ref.[1]. The quantum telegraph noise is described by a impurity level tunnel coupled to a non-interacting electron reservoir. The qubit is coupled to the fluctuating charge $Q = d^\dagger d$ of the impurity. The normal-ordered Hamiltonian of the entire system is

$$H = \frac{\Delta}{2}\sigma_z + \frac{1}{2}\vec{v} \cdot \vec{\sigma} \cdot d^\dagger d + \epsilon_d d^\dagger d + \sum_k \left(t_k c_k^\dagger d + t_k^* d^\dagger c_k \right) + \sum_k \epsilon_k c_k^\dagger c_k. \quad (2.1)$$

Here c_k^\dagger creates an electron of energy ϵ_k in the bath and d^\dagger creates an electron on the impurity level of energy ϵ_d . With the tunneling amplitude t_k between the impurity and a bath level of energy ϵ_k the tunneling rate γ can be written as:

$$\gamma = 2\pi \sum_k \|t_k\|^2 \delta(\epsilon_k - \epsilon_d). \quad (2.2)$$

The tunneling rate is also the spectral broadening of the impurity level. Since the fluctuation rate of the charge of the impurity as well as the coupling strength \vec{v} between impurity and qubit are changing noise characteristics, the strength of the noise can be expressed with $\frac{\vec{v}}{\gamma}$.

2.2 The Master Equation

We analyze the time evolution of the qubit exposed to QTN by deriving a Markovian quantum master equation. The steps performed here follow in general Ref.[4], Ref.[6, Ch.3.3.1] and they are also presented in Ch.A.1.1. The Hamiltonian of Eq.2.1 will be split

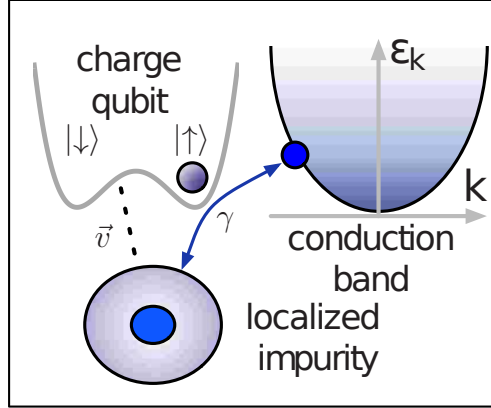


Figure 2.1: Schematic picture of the quantum telegraph noise model from Ref.[1].

into H_0 and the interaction Hamiltonian H_I

$$\begin{aligned}
 H_0 &= \frac{\Delta}{2}\sigma_z + \epsilon_d d^\dagger d + \sum_k \left(t_k c_k^\dagger d + t_k^* d^\dagger c_k \right) + \sum_k \epsilon_k c_k^\dagger c_k, \\
 H_I &= \frac{1}{2} \vec{v} \cdot \vec{\sigma} \cdot d^\dagger d = A \otimes B.
 \end{aligned} \tag{2.3}$$

After applying the projection operator method, the dynamics of the qubit $\dot{\rho}_S(t)$ can be expressed with its interaction picture density matrix $\dot{\tilde{\rho}}_S(t)$

$$\begin{aligned}
 \dot{\rho}_S(t) &= -i[H_0, \rho_S(t)] + U_0(t) \dot{\tilde{\rho}}_S(t) U_0^\dagger(t), \\
 \dot{\tilde{\rho}}_S(t) &= -\alpha^2 \int_0^\infty ds \text{tr}_B \left[\tilde{H}_I(t), \left[\tilde{H}_I(t-s), \tilde{\rho}_S(t) \otimes \rho_B \right] \right].
 \end{aligned} \tag{2.4}$$

For the second relation two important approximations were made. The Born approximation assumes a weak coupling between bath and qubit such that the influence of the qubit on the bath being in a thermal equilibrium state is very small leading to the time evolution $\rho(t) \approx \rho_S(t) \otimes \rho_B$ of the entire system. Additionally the Markov approximation presumes that the system has no memory. This is a good approximation when excitations of the bath decay very fast compared to the intrinsic time evolution of the qubit.

We decompose the interaction Hamiltonian with eigenoperators Π of $H_S = \frac{\Delta}{2}\sigma_z$

$$\begin{aligned}
 \Pi \left(\frac{\Delta}{2} \right) &= |1\rangle \langle 1|, \\
 \Pi \left(-\frac{\Delta}{2} \right) &= |0\rangle \langle 0|,
 \end{aligned} \tag{2.5}$$

to simplify the calculation of \tilde{H}_I .

$$\begin{aligned} A(\Delta) &= \Pi\left(-\frac{\Delta}{2}\right) A \Pi\left(\frac{\Delta}{2}\right) = \frac{1}{2}(v_x - iv_y)\sigma^-, \\ A(-\Delta) &= \Pi\left(\frac{\Delta}{2}\right) A \Pi\left(-\frac{\Delta}{2}\right) = \frac{1}{2}(v_x + iv_y)\sigma^+, \\ A(0) &= \Pi\left(-\frac{\Delta}{2}\right) A \Pi\left(-\frac{\Delta}{2}\right) + \Pi\left(\frac{\Delta}{2}\right) A \Pi\left(\frac{\Delta}{2}\right) = \frac{1}{2}v_z\sigma_z. \end{aligned} \quad (2.6)$$

According to Eq.A.22 the interaction picture Hamiltonian is then

$$\tilde{H}_I(t) = (e^{-i\Delta t}A(\Delta) + e^{i\Delta t}A(-\Delta) + A(0)) \otimes \tilde{B}(t). \quad (2.7)$$

This expression can be inserted in Eq.2.4 and simplified to

$$\begin{aligned} \frac{d}{dt}\tilde{\rho}_S(t) &= \sum_{\omega, \omega'} e^{i(\omega' - \omega)t} \Gamma(\omega) (A(\omega)\tilde{\rho}_S(t)A^\dagger(\omega') - A^\dagger(\omega')A(\omega)\tilde{\rho}_S(t)) + h.c., \\ \text{with } \Gamma(\omega) &= \int_0^\infty ds e^{i\omega s} \langle \tilde{B}^\dagger(t)\tilde{B}(t-s) \rangle_{\rho_B}, \\ \text{and } \omega &\in \{-\Delta, 0, \Delta\}. \end{aligned} \quad (2.8)$$

A further simplification needs a secular approximation which ignores exponentials with non-vanishing exponents. This is only applicable if the time scale about which the qubit evolves $\tau_S \sim \frac{1}{\Delta}$ is large compared to its relaxation time τ_R together with overall faster decaying bath correlation functions $\tau_B = \frac{1}{\gamma}$. Therefore the following part is only reasonable for at least $\Delta < \gamma$, a condition already needed for the Markov approximation. Under this approximation, terms with $\omega' \neq \omega$ can be neglected

$$\frac{d}{dt}\tilde{\rho}_S(t) = \sum_{\omega} \Gamma(\omega) (A(\omega)\tilde{\rho}_S(t)A^\dagger(\omega) - A^\dagger(\omega)A(\omega)\tilde{\rho}_S(t)) + h.c.. \quad (2.9)$$

By splitting $\Gamma(\omega)$ into real and imaginary parts

$$\Gamma(\omega) = \frac{1}{2}\gamma(\omega) + iS(\omega), \quad (2.10)$$

$$\gamma(\omega) = \int_{-\infty}^\infty ds e^{i\omega s} \langle \tilde{B}^\dagger(t)\tilde{B}(t-s) \rangle_{\rho_B}, \quad (2.11)$$

Eq.2.9 can be brought to Lindblad form

$$\frac{d}{dt}\tilde{\rho}_S(t) = \sum_{\omega} \gamma(\omega) L[A(\omega)]\tilde{\rho}_S(t) - \sum_{\omega} iS(\omega) [A^\dagger(\omega)A(\omega), \tilde{\rho}_S(t)], \quad (2.12)$$

where the Lindblad superoperator acting on a density matrix was used:

$$L[A]\rho = A\rho A^\dagger - \frac{1}{2}\{A^\dagger A, \rho\}. \quad (2.13)$$

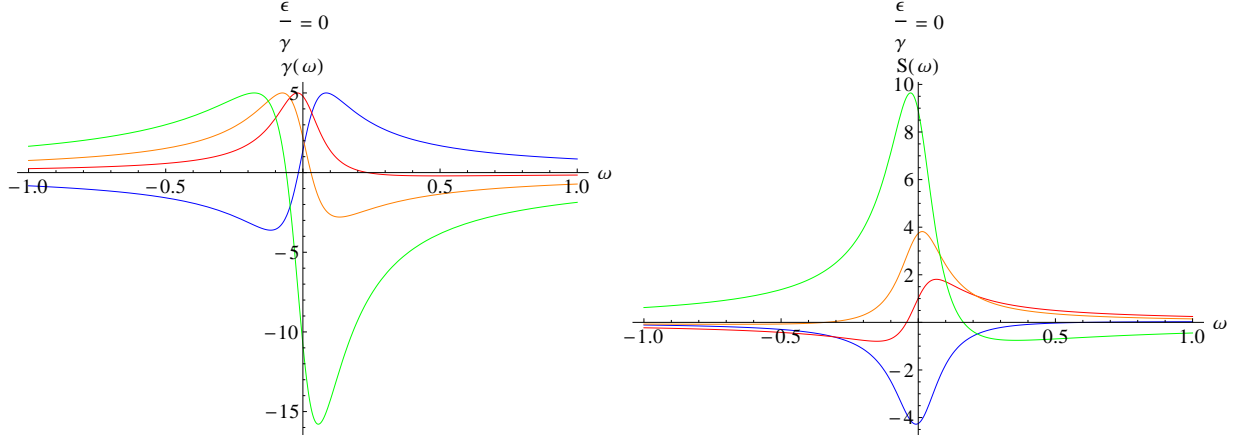


Figure 2.2: The functions $\gamma(\omega)$ (left) and $S(\omega)$ (right) for $\gamma = 0.1$, $\epsilon_d = 0$ and $\frac{T}{\gamma} = 0.065, 0.085, 0.1, 0.12$ (blue, red, orange, green).

It is important to note that $\gamma(\omega) \neq \gamma$, but the notation was used for a better agreement with the literature. At this point the one-sided Fourier transform $\Gamma(\omega)$ of the correlation function, $\gamma(\omega)$ and $S(\omega)$ still have to be calculated explicitly to obtain a relation between the properties of the QTN and the time evolution of the qubit. This is done in detail in Ch.A.1.3 and a numerical evaluation of $\gamma(\omega)$ and $S(\omega)$ is shown in Fig.2.2. Both functions exhibit no remarkable symmetry in general. If we expand the sums in Eq.2.12 we can identify different terms

$$\begin{aligned} \frac{d}{dt} \tilde{\rho}_S(t) &= \gamma(0) \frac{v_z^2}{4} \underbrace{L[\sigma_z] \tilde{\rho}_S(t)}_{\text{dephasing}} + \frac{v_x^2 + v_y^2}{4} (\gamma(-\Delta) \underbrace{L[\sigma^+] \tilde{\rho}_S(t)}_{\text{incoherent pumping}} + \gamma(\Delta) \underbrace{L[\sigma^-] \tilde{\rho}_S(t)}_{\text{decay}}) \\ &\quad - i [H_{LS}, \tilde{\rho}_S(t)], \end{aligned} \quad (2.14)$$

$$H_{LS} = (S(\Delta) |1\rangle \langle 1| + S(-\Delta) |0\rangle \langle 0|) \frac{v_x^2 + v_y^2}{4}.$$

As indicated above, the terms are known to be responsible for decoherence by pure dephasing, incoherent pumping and decay. The last term with H_{LS} is known as the Lamb shift giving a contribution to the energy level spacing of the qubit. Both functions $\gamma(\omega)$ and $S(\omega)$ depend on the temperature $T = \frac{1}{\beta}$, the energy level of the impurity ϵ_d and on the tunneling rate γ . As described in the next section 2.3.1, these parameters will be fixed for further calculations meaning that $\gamma(0)$, $\gamma(\pm\Delta)$ and $S(\pm\Delta)$ can be treated as constants. Thus the rates $\Gamma_\uparrow = \gamma(-\Delta) \frac{v_x^2 + v_y^2}{4}$, $\Gamma_\downarrow = \gamma(\Delta) \frac{v_x^2 + v_y^2}{4}$ and the dephasing rate $\Gamma_\varphi = \gamma(0) \frac{v_z^2}{4}$ only depend on the specific coupling to the noise. This derivation shows that the quantum master equation can be generally written in terms of

$$\dot{\rho}_S(t) = -i[H_0 + H_{LS}, \rho_S(t)] + \Gamma_\uparrow L[\sigma^+] \rho_S(t) + \Gamma_\downarrow L[\sigma^-] \rho_S(t) + \Gamma_\varphi L[\sigma_z] \rho_S(t). \quad (2.15)$$

It has to be kept in mind that this equation was derived for $\Delta < \gamma$ as well as a weak coupling between bath and qubit and is not valid anymore for stronger couplings, especially for those

which are examined in the next section exhibiting special properties of QTN.

2.3 DMRG and Model Parameters

As described in Ref.[14, 8] the bath-impurity part of the Hamiltonian will be mapped onto a Wilson chain which is mathematically a tridiagonalization of the Hamiltonian. The ground state of the Wilson chain form Hamiltonian can be calculated using infinite and finite DMRG [29]. Afterwards the time evolution of the starting state can be performed using t-DMRG.

The quality of the results and their agreement with real systems depend very much on the particular choice of bath discretization. Additionally a proper selection of model parameters is important as for certain ranges of values the characteristics of QTN is similar to Gaussian noise which is not desired. Such parameters are half bandwidth D , impurity energy level ϵ_d , qubit energy level spacing Δ and electron transition rate γ . As reference the analytical results in Fig.2.3 of Benjamin Abel Ref.[2, ch.7] will be used.

2.3.1 D , Δ , γ and ϵ_d

The first value to be set is the half bandwidth of the reservoir. We chose $D = 1$ as the energy scale of our model. The bath contains spinless fermions and is half filled. In the starting state at $T = 0$ the highest occupied bath level is the level of Fermi energy $\epsilon_F \approx 0$. Its value depends in the simulations on the bath discretization and should be ideally zero. By varying the impurity energy level ϵ_d with respect to ϵ_F the fluctuation rate of the QTN can be adjusted. If we choose $\epsilon_d > \epsilon_F$ the impurity will be more rarely occupied whereas for $\epsilon_d < \epsilon_F$ it will be more likely to be occupied. Thus the hopping rate in these cases will be lower than for $\epsilon_d \approx \epsilon_F$. Since higher fluctuations lead to stronger decoherence effects, a good choice is $\epsilon_d = 0$. The properties of other values are analyzed in Ref.[2, ch.7.4]. According to Ref.[1] the tunneling rate should be smaller than half bandwidth $\gamma \ll D$ and it is used in $\frac{v_z}{\gamma}$ as a measure for the strength of the noise. Hence $\gamma = 0.1$ was an appropriate choice. The qubit level spacing Δ was set to 0.2, but computations showed that this parameter does not influence results of free decoherence of the qubit.

2.3.2 Discretization and Bath Length

The fermionic bath can be discretized either linearly or logarithmically each with its own advantages. We need a high density of states around Fermi energy level because most transitions will happen there for low temperatures $T \rightarrow 0$. At the same time a small bath length L is desired to have a short computation time. To assess the accuracy of simulations for different parameter choices, the visibility $|D(t)|$ of the qubit will be used as a benchmark. As the qubit is initially prepared in an eigenstate of σ_x and coupled with $v_x = 0, v_y = 0, v_z = 0.3$ to the impurity, the t-DMRG results should be similar to the red curve in Fig.2.3. The reference plot shows a good QTN characteristic with a zero crossing

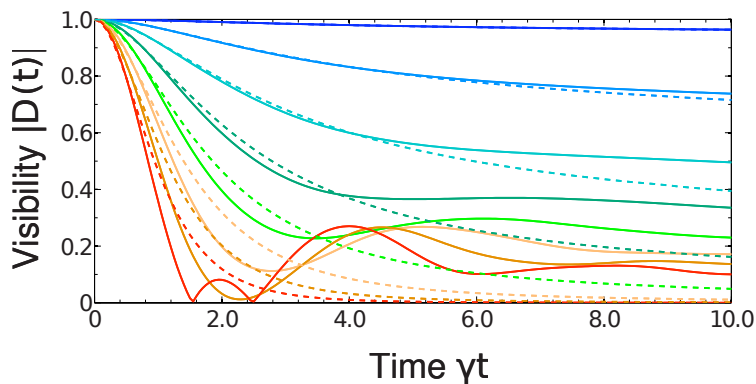


Figure 2.3: Analytical results for $|D(t)|$ for couplings $\frac{v}{\gamma} = 0.2, 0.6, 1.0, 1.4, 1.8, 2.2, 2.6, 3.0$ (from top to bottom). Dashed lines show the Gaussian approximation. The red curve exhibits a first zero crossing at $\gamma t \approx 1.6$. Figure from Ref.[1].

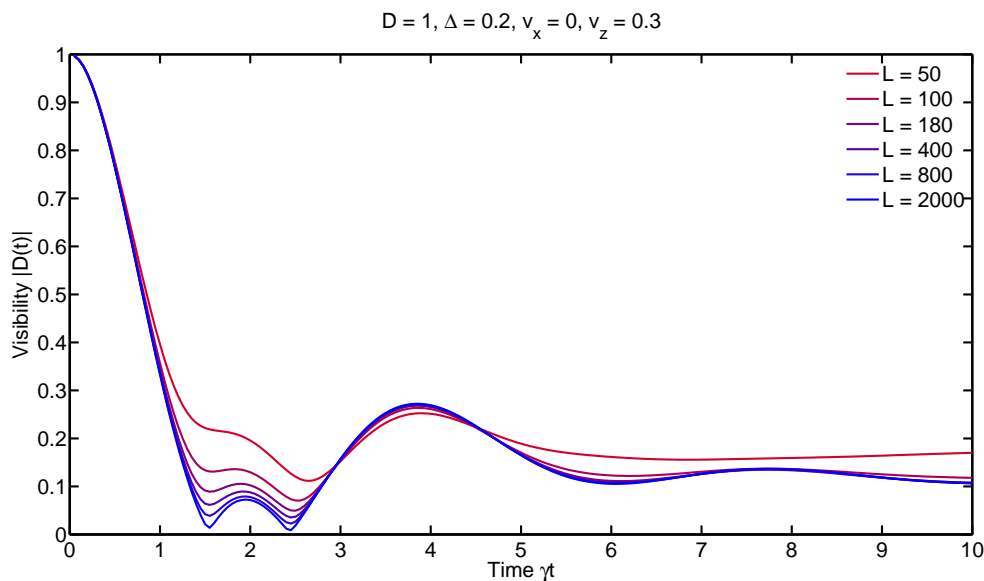


Figure 2.4: Comparison of visibility $|D(t)|$ for different bath lengths L with linear discretization and $\frac{v}{\gamma} = 3$. Long time behavior $\gamma t > 3$ converges fast, but first zero crossing very slowly.

at $\gamma t \approx 1.6$ and a non-vanishing visibility for long times $\gamma t = 10$.

The linear discretization divides the bath into equidistant discrete energy levels

$$\epsilon_0 = 0, \epsilon_k = (2k - 1) \cdot \frac{D}{L}, \quad \text{with } k \in \left\{ -\frac{L}{2}, \dots, \frac{L}{2} \right\}. \quad (2.16)$$

To get accurate results this type needs a very high number of sites L , see Fig.2.4. While for $\gamma t > 3$, $|D(t)|$ is already very good for $L = 100$, the zero crossing is not even reached for $L = 2000$ and converges very slowly. As mentioned in Ref.[2] the first zero crossing depends on temperature T , coupling v_z and on the difference between ϵ_d and ϵ_F . As $\epsilon_d = 0, T = 0$ and $v_z = 0.3$, this gives rise to the conjecture that $\epsilon_d \neq \epsilon_F \neq 0$ which is an effect of the particular implementation of the linear discretization.

The logarithmic discretization

$$\epsilon_0 = 0, \quad \epsilon_{\pm 1} = \pm D \left(\frac{1 - \frac{1}{\Lambda}}{\ln \Lambda} + 1 - z \right), \quad (2.17)$$

$$\epsilon_{\pm k} = \pm D \frac{1 - \frac{1}{\Lambda}}{\ln \Lambda} \Lambda^{2-k-z}, \quad \text{with } k \in \left\{ 2, \dots, \frac{L}{2} \right\}, \quad (2.18)$$

is defined through its parameter Λ . By increasing Λ the resolution around ϵ_F is enhanced and less important high energy levels are removed. Thus the first zero crossing in Fig.2.5 converges much faster than in the linear case. While even at small bath lengths results are very accurate for $\gamma t < 3$, oscillatory errors occur for longer times. These strong artificial oscillations of the visibility are a consequence of the removal of higher energy levels, as in the time scope of $\gamma t > 3$ these energy levels become important. A method to compensate this error is to introduce the additional level shift parameter z and to average over calculations for different values of $z \in]0, 1]$. As shown in Fig.2.6 the oscillations are very regular such that for an equidistant choice of z the z -averaged result is very accurate. Besides the computation of less sites this method has also the advantage of parallel computing speeding up calculations tremendously.

We found that a very good choice was $\Lambda = 1.8$, $L = 34$, $z \in \left\{ \frac{1}{8}, \dots, 1 \right\}$. A further increase of Λ and decrease of L effected only additional errors and less benefit of computation time. By way of comparison, the simulation of the z -averaged curve in Fig.2.6 took about 1 minute whereas the $L = 2000$ one needed 1 hour on a single cpu core.

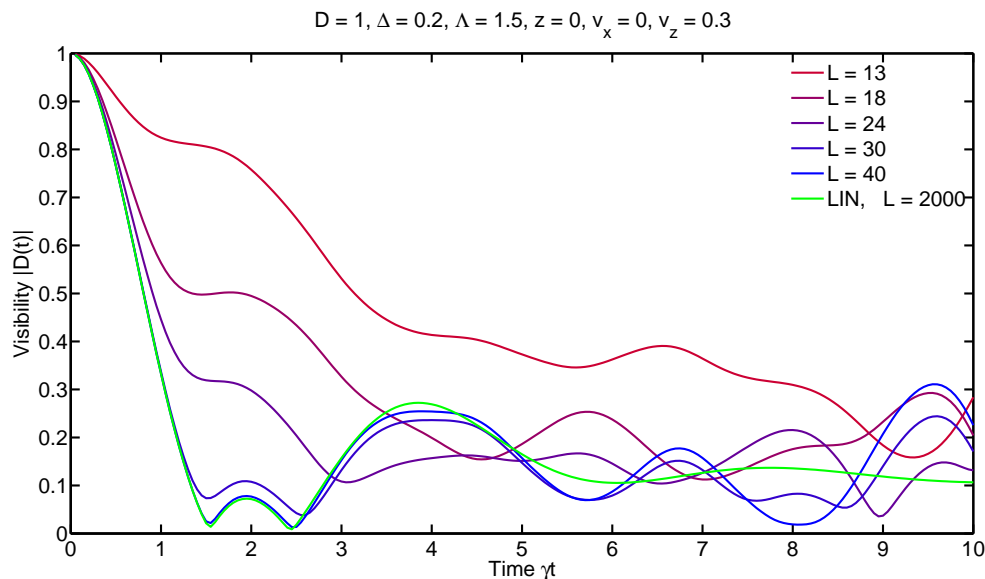


Figure 2.5: Comparison of visibility $|D(t)|$ for different bath lengths L with logarithmic discretization and $\frac{v}{\gamma} = 3$. First zero crossing converges fast, but long time behavior exhibits errors.

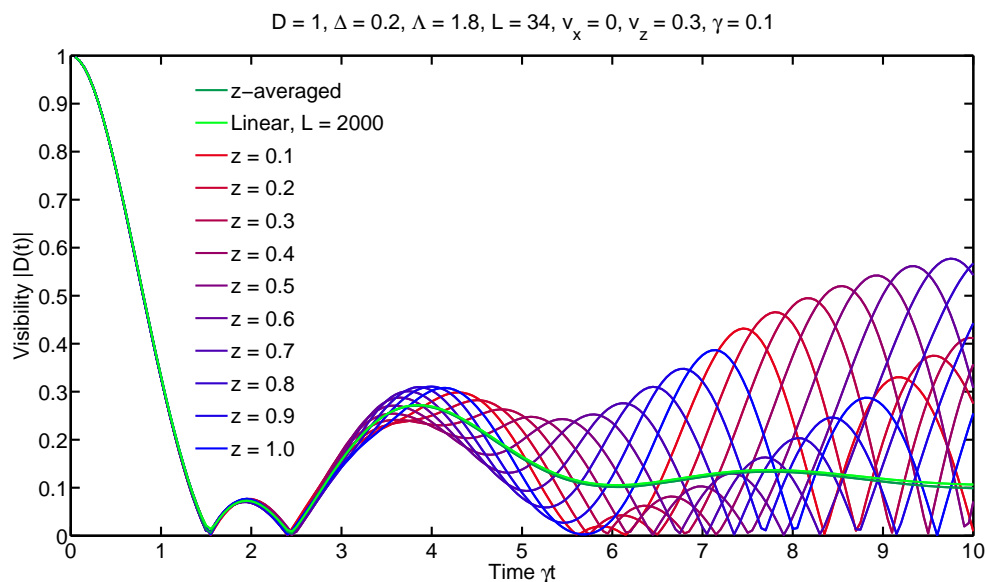


Figure 2.6: Method of z -averaging for logarithmic discretization. Visibility oscillations for $\gamma t > 3$ (blue to red) are caused by bad high energy resolution. Averaged result (dark green) is very close to almost exact result from linear bath with $L = 2000$ (light green).

Chapter 3

The Periodically Driven Qubit

In quantum optics and quantum information processing a frequently used technique to manipulate qubits is the application of π -pulses. With this tool it is possible to exactly control the state of a qubit by using certain pulse protocols like spin echo [21] or bang-bang [15]. These protocols can be used to recover quantum information which degenerates as the qubit loses its coherence through unavoidable interactions with its environment. However the precision of the pulse manipulations is also affected by the external noise and the effect is not easy to describe analytically. Hence it will be simulated and analyzed in this chapter.

3.1 The Full Model

The external driving field representing the pulses is added to the Hamiltonian of the QTNM

$$H = \frac{\Delta}{2}\sigma_z + \frac{1}{2}\vec{v}\vec{\sigma} \cdot d^\dagger d + \epsilon_d d^\dagger d + \sum_k \left(t_k c_k^\dagger d + t_k^* d^\dagger c_k \right) + \sum_k \epsilon_k c_k^\dagger c_k + \Omega \cos(\omega_d t) \sigma_x. \quad (3.1)$$

The field with amplitude Ω and driving frequency ω_d is treated here in a classical way since it is simple to implement and correct for classical fields. Hence the interaction between qubit and field in absence of the QTN will be handled in a semi-classical way in the following section 3.2 and explicitly calculated in Ch.A.3. An alternative fully quantum mechanical description by the Jaynes-Cummings-Hamiltonian is presented in Ch.A.4. Afterwards the effect of the QTN will be analyzed in Ch.3.4 and pulse protocols will be simulated in Ch.3.5.

3.2 Rabi Oscillations

When a two-level system is transverse coupled to an external oscillating field, its probability of being found in one of its two states will perform oscillations between $[0, 1]$ with a certain transition frequency (see Fig.3.1). These Rabi oscillations can be described with

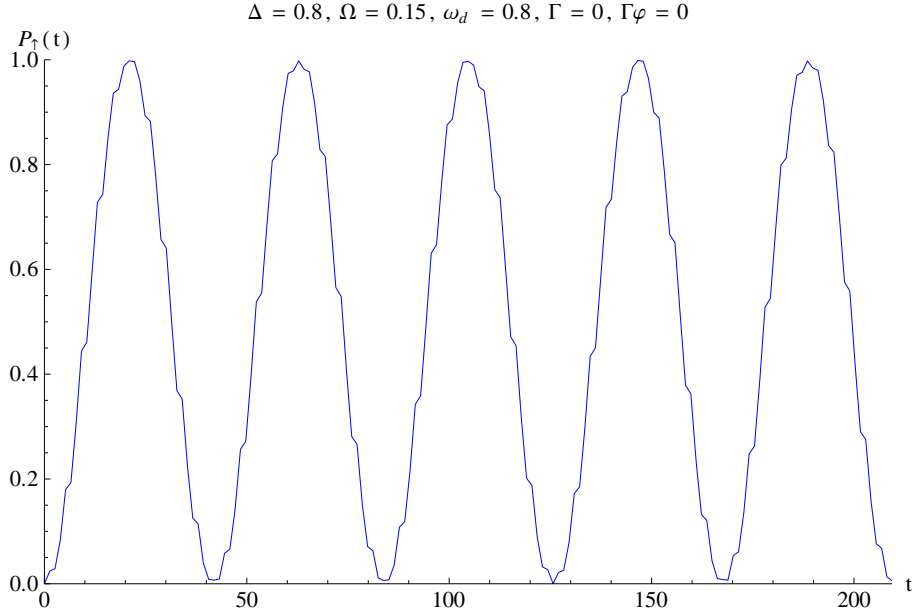


Figure 3.1: Rabi oscillations of the probability of the excited state $P_{\uparrow}(t)$ for strong driving. The Rabi oscillations become smooth in the case of a weak driving.

the Hamiltonian of the qubit-field interaction

$$H = \frac{\Delta}{2}\sigma_z + \Omega \cos(\omega_d t)\sigma_x, \quad (3.2)$$

with the Rabi frequency Ω and driving frequency ω_d . The Rabi problem is usually calculated under the Rotating-Wave-Approximation (RWA) where the driving amplitude is assumed to be weak $\Omega \ll \Delta$. The explicit derivation in Ch.A.3.1 shows that the transition frequency, called the generalized Rabi frequency Ω' is:

$$\Omega' = \sqrt{\Omega^2 + (\Delta - \omega_d)^2}. \quad (3.3)$$

We can see that Ω' is minimized and equals Ω only at a resonant driving ($\Delta = \omega_d$). The Rabi oscillation of the qubit's probability $P_{\uparrow}(t)$ of the excited state is given by

$$P_{\uparrow}(t) = \frac{\Omega^2}{\Omega'^2} \sin^2\left(\frac{\Omega' t}{2}\right) = \frac{1}{2} \frac{1}{1 + \left(\frac{\Delta - \omega_d}{\Omega}\right)^2} (1 - \cos(\Omega' t)), \quad (3.4)$$

where we used the initial conditions $P_{\uparrow}(0) = 0, P_{\downarrow}(0) = 1$. Here it can be seen that the amplitude depends on the detuning $\Delta - \omega_d$ as well as on the driving strength Ω and it is maximized for a resonant driving. In Fig.3.1 Rabi oscillations and their spectrum in Fig.3.2 are plotted in the case of a strong driving. We can see the predominant Rabi oscillation with frequency Ω' between $[0, 1]$ as well as smaller higher order oscillations of 2ω called

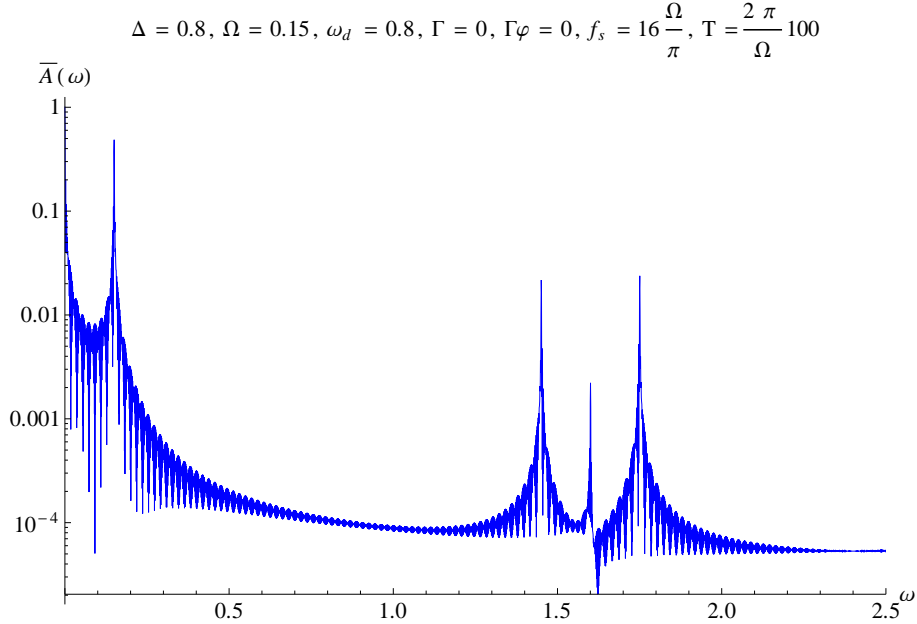


Figure 3.2: Spectrum of $P_{\uparrow}(t)$ obtained via discrete Fourier transform with zero padding. The peak to the left is the Rabi peak at Ω' . The three peaks in the middle are the Bloch-Siegert oscillations at $2\omega_d - \Omega'$, $2\omega_d$, $2\omega_d + \Omega'$.

Bloch-Siegert oscillations [30]. These Bloch-Siegert oscillations and weaker higher order generalized Bloch-Siegert oscillations (GBSO) at frequencies of multiples of 2ω cannot be calculated with the RWA [24]. Although these GBSOs are weak compared to the main Rabi oscillation, they become stronger at higher amplitudes Ω and make it difficult to perform exact Qubit manipulations.

3.2.1 Pulses

Based on Rabi oscillations, the state of a qubit can be controlled very accurately with pulses defined by

$$\begin{aligned} \pi - \text{Pulse} : \quad \Omega't &= \pi, \\ \frac{\pi}{2} - \text{Pulse} : \quad \Omega't &= \frac{\pi}{2}. \end{aligned} \tag{3.5}$$

With these definitions a π -pulse flips the qubit from ground to excited state whereas a $\frac{\pi}{2}$ -pulse brings it from the ground state into a σ_y eigenstate. Using the Bloch vector representation a π -pulse rotates the Bloch vector by 180° around the x -axis and a $\frac{\pi}{2}$ -pulse by 90° .

Additionally π -pulses can be performed in different ways, either strong and short in duration, or weak but long. Considering the QTN it might be desirable to perform pulses which

are relative short compared to the fluctuation rate of the QTN in order to get distortion-free manipulations. Hence it is necessary to study the effect of strong driving fields.

3.3 Bloch-Siegert Shift

In the strong driving regime $\frac{\Omega}{\Delta} > 0.1$ the Bloch-Siegert shift of the resonance frequency to values greater than Δ is observable [3, 5, 31]. This shift is relevant for accurate pulses as it leads to a change of Ω' (see Fig.3.4). The Bloch-Siegert shift can be derived from the Schrödinger equation by doing an assumption different from the RWA (explicitly in Ch.A.3.2). In the RWA time scales given by the weak driving $\Omega \ll \Delta$ were considered and rapidly oscillating terms with $e^{\pm i(\Delta+\omega_d)t}$ were averaged out. But as driving becomes stronger these terms give contribution to the qubit's energy level splitting in form of a level shift λ_+ . Therefore the corrected qubit energy Δ'_{BS} respecting the Bloch-Siegert shift can be calculated to

$$\lambda_{\pm} = -\frac{\Delta + \omega_d}{2} \pm \frac{1}{2} \sqrt{(\Delta + \omega_d)^2 + \Omega^2}, \quad (3.6)$$

$$\Delta'_{BS} = \Delta + 2\lambda_+ = -\omega_d + \sqrt{(\Delta + \omega_d)^2 + \Omega^2}. \quad (3.7)$$

A resonant driving is now obtained via $\omega_d = \Delta'_{BS} =: \omega_{BS}$ and the resonance condition for ω_{BS} is:

$$\omega_{BS} = \frac{1}{2} \sqrt{(\Delta + \omega_{BS})^2 + \Omega^2}, \quad (3.8)$$

$$\omega_{BS} = \Delta \left(\frac{1}{3} + \frac{2}{3} \sqrt{1 + \frac{3\Omega^2}{4\Delta^2}} \right) \quad (3.9)$$

$$\stackrel{\Omega < \Delta}{\simeq} \Delta \left(1 + \frac{\Omega^2}{4\Delta^2} \right), \quad (3.10)$$

$$\Rightarrow \Delta\omega_{BS} \simeq \frac{\Omega^2}{4\Delta}. \quad (3.11)$$

Here the last expression is the approximated Bloch-Siegert shift of the qubit energy-level splitting in case of resonant driving and $\Omega < \Delta$.

3.3.1 Finding the Bloch-Siegert Shift

To confirm the Bloch-Siegert shift, two ways of finding the resonance might be used. The first one is to search for the maximum amplitude of the Rabi oscillations with respect to different driving frequencies. Another possibility is to vary ω_d and search for a minimum in the position of the generalized Rabi frequency Ω' . As both methods analyze the peak of the Rabi oscillations Ω' in the spectrum, the discrete Fourier transformation (DFT) used here is explained in Ch.A.2.

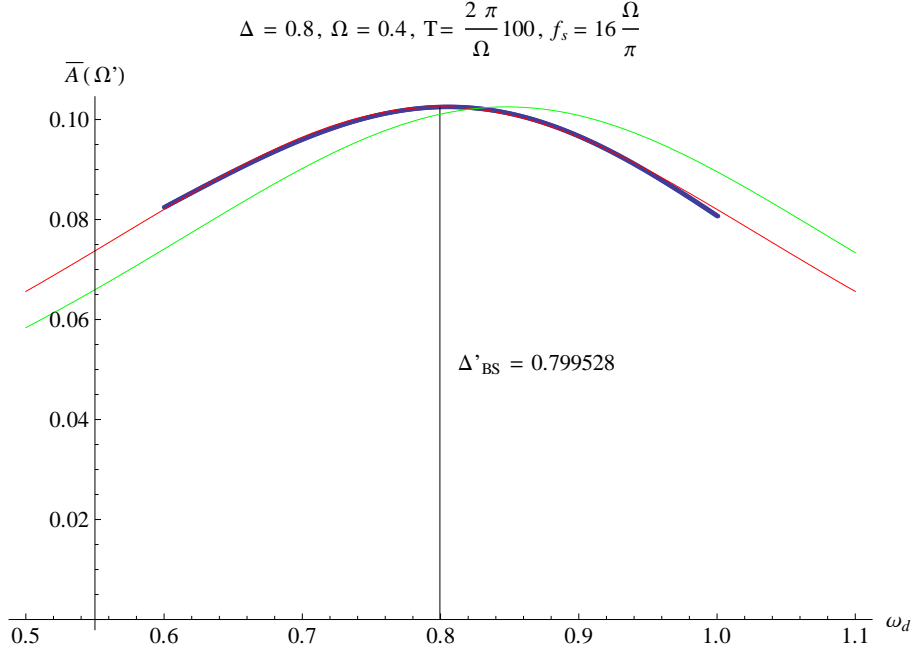


Figure 3.3: Averaged amplitudes $\bar{A}(\Omega')$ of Rabi oscillations Ω' for driving frequencies ω_d (blue) calculated with a flat-top windowed DFT. The vertical line marks the maximum amplitude found and the Δ' obtained via fitting Eq.3.12. The green curve shows expected values calculated with Eq.3.12, whereas the red curve accords to the amplitude without modification. With Eq.3.9 calculated value of resonance frequency: $\omega_{BS} = 0.847853$.

Evaluating Rabi Amplitude

The assumption made in this method was that the corrected energy level spacing of the qubit Δ'_{BS} from the Bloch-Siegert shift could be inserted into Eq.3.4 leading to a corrected behaviour of the amplitudes

$$A_{BS}(\omega_d) = \frac{1}{2} \frac{1}{1 + \left(\frac{\Delta' - \omega_d}{\Omega}\right)^2}. \quad (3.12)$$

The peak values $\bar{A}(\Omega')$ were measured for different driving frequencies ω_d . In Fig.3.3 these peak values are compared with the predicted amplitude behavior (green) and the original one (red). It was assumed that the resonant driving $\omega_d = \Delta'$ could be found by searching for the maximum $\bar{A}(\Omega')$. The assumption does obviously not hold as resonance is in this case at $\omega_{BS} = 0.847853$ and the amplitude is maximized for $\omega_d = 0.799528$.

The measurements were performed using zero-padding and a flat-top window in the DFT. This DFT method has very small errors in measuring peak amplitudes and should be very accurate. But as amplitudes are not shifting, the assumption leading to Eq.3.12 has to be wrong and cannot be used to measure the resonance frequency and Bloch-Siegert shift.

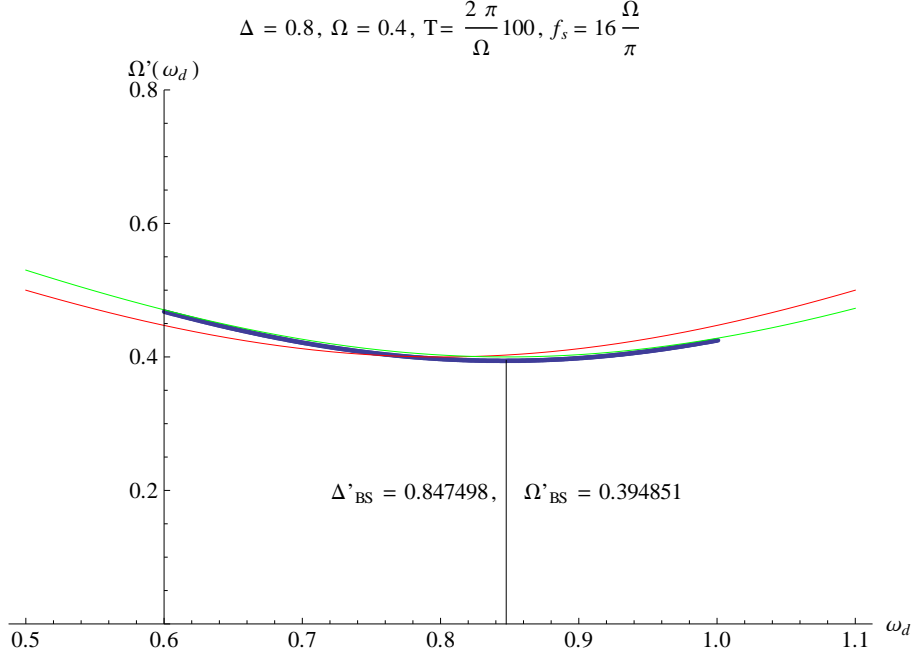


Figure 3.4: Plot shows the measured generalized Rabi frequency Ω' for driving frequencies ω_d (blue). The minimum is reached for resonant driving $\omega_d = \Delta'_{BS}$, which is marked by the line. Comparison with theoretical curves from Eq.3.13(green) and Eq.3.3(red) show that the shift is measurable. Expected: $\omega_{BS} = 0.847853$.

Evaluating Rabi Frequency

Similar to the first method, a corrected generalized Rabi frequency Ω'_{BS} is obtained by taking Eq.3.3 and replacing Δ with the corrected Δ'_{BS} .

$$\Omega'_{BS} = \sqrt{\Omega^2 + (\Delta'_{BS} - \omega_d)^2} = \sqrt{\Omega^2 + (\Delta - \omega_d + 2\lambda_+)^2}. \quad (3.13)$$

From this equation we see that the generalized Rabi frequency is minimized at the shifted resonance $\omega_d = \Delta'_{BS}$. This also means that Ω'_{BS} is simply shifted by $2\lambda_+$ compared to Ω' . In Fig.3.4 the measured Rabi peak frequencies $\Omega'(\omega_d)$ for different ω_d are compared to the original (red) and corrected (green) formula for the generalized Rabi frequency. The plot exhibits a very good agreement between the measurements and Eq.3.13 with a relative error of 4×10^{-4} and assures that the replacement of Δ with Δ'_{BS} in this case is legitimate.

Using the second method, we can confirm Eq.3.9 of the Bloch-Siegert shift as shown in Fig.3.5. The measured and exact values agree in the range $\frac{\Omega}{\Delta} < 0.5$. The measurements at $\frac{\Omega}{\Delta} > 0.5$ have errors as the curve in Fig.3.4 flattens, thus making the curve fitting inaccurate. Overall we confirmed that the evaluation of Rabi frequency presented here can be used to find the resonance frequency and to analyze the effect of QTN in t-DMRG simulations.

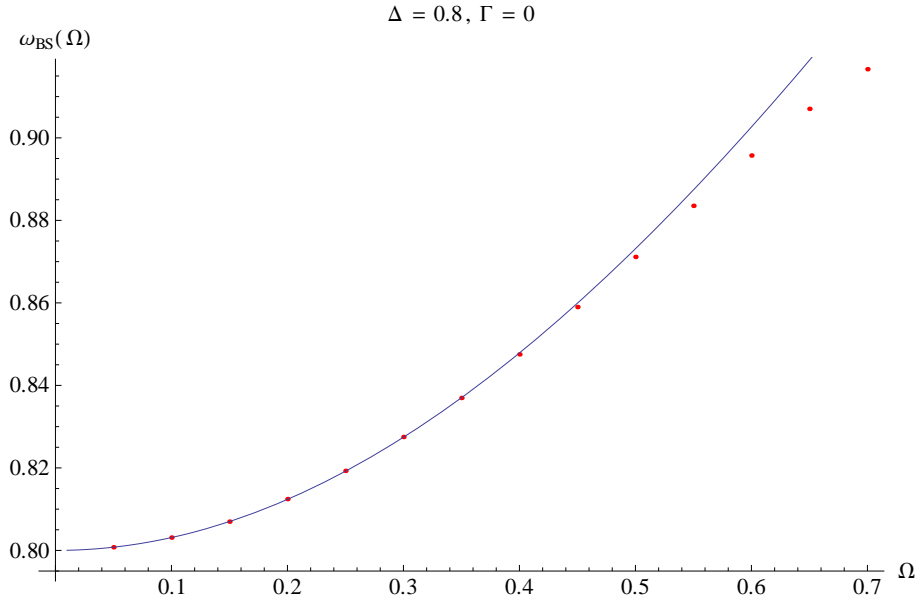


Figure 3.5: Comparison of the measured Bloch-Siegert shift (red) and the exact solution (blue) of Eq.3.9.

3.4 Driven Qubit Coupled to QTN

To properly understand the effect of QTN on pulses, its influence on Rabi oscillations is studied here. Simulations were done with a qubit, initially prepared in the ground state $|0\rangle$ under weak and resonant driving $\frac{\Omega}{\Delta} = 0.02$. We tested longitudinal $\frac{v_z}{\gamma} = 1$ and transverse $\frac{v_x}{\gamma} = 1$ coupling to the bath. From Fig.3.6 it can be seen that the $v_z \gg \Omega$ coupled QTN inhibits resonant Rabi oscillations, but adds no damping. The green line oscillates with a frequency of $\Omega' = 0.0485$ and has a maximum excitation of $P_{\uparrow, max} = 0.03$. This result can be explained as the qubit's energy level splitting is modified by the fluctuating charge:

$$\frac{\tilde{\Delta}}{2}\sigma_z = \left(\frac{\Delta}{2} + \frac{v_z}{2}d^\dagger d \right) \sigma_z, \quad (3.14)$$

where $Q = d^\dagger d$ equals 1 if an electron occupies the impurity and 0 otherwise. In contrast to the situation of $Q = 0$ where $\Omega' = \Omega$ and $P_{\uparrow, max} = 1$, the case $Q = 1$ leads to modifications because of a detuned driving $\delta = \tilde{\Delta} - \omega = v_z$:

$$\begin{aligned} \tilde{\Omega}' &= \Omega \sqrt{1 + \left(\frac{v_z}{\Omega} \right)^2}, \\ \tilde{P}_{\uparrow, max} &= 2\tilde{A}(\tilde{\Omega}) = \frac{1}{1 + \left(\frac{v_z}{\Omega} \right)^2}. \end{aligned} \quad (3.15)$$

If we calculate these quantities according to the simulation in Fig.3.6, we get $\tilde{\Omega}' \approx 0.1$ and $\tilde{P}_{\uparrow, max} \approx 0.01$. The values measured in the simulation are right between the calculations

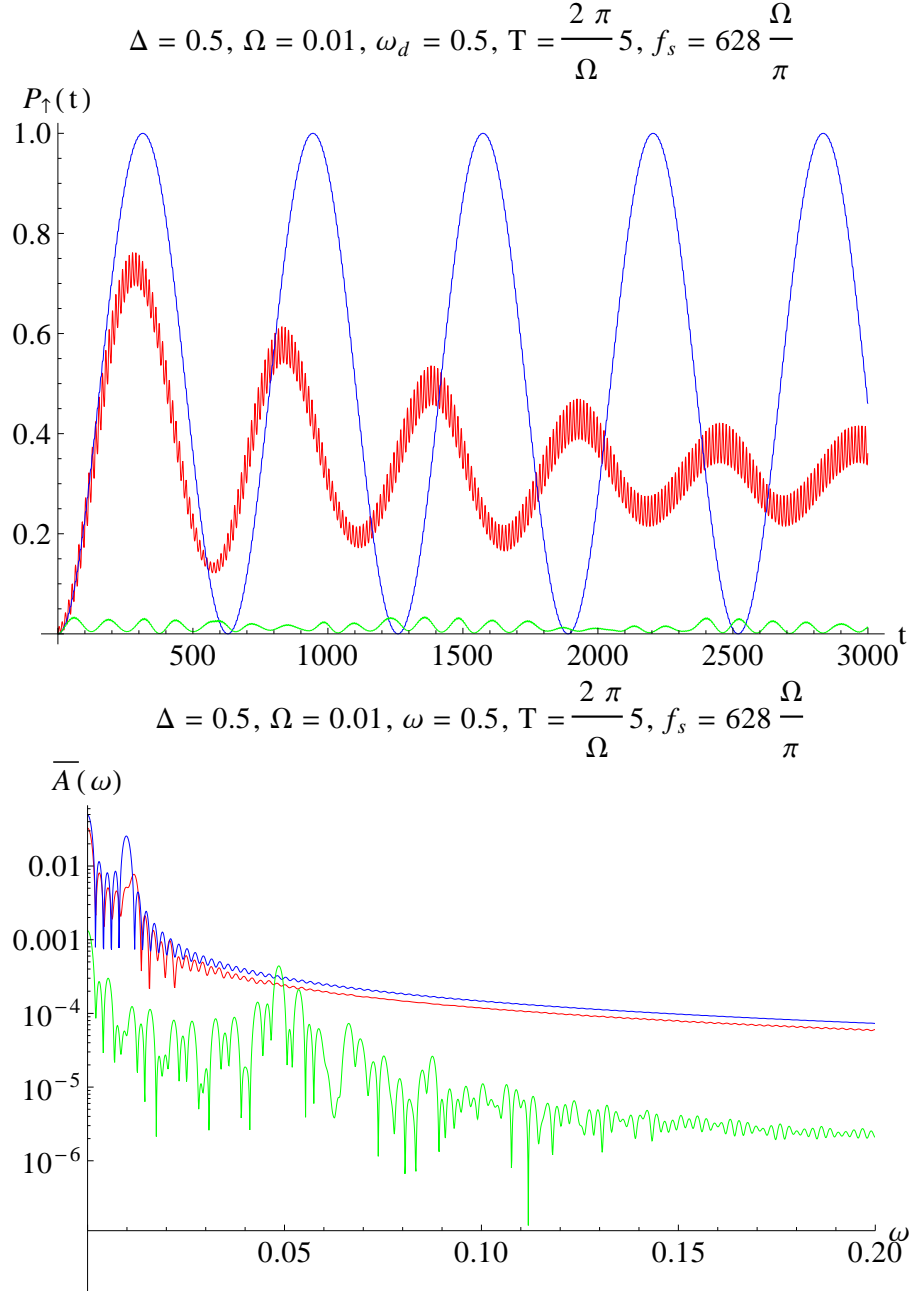


Figure 3.6: Different couplings to QTN with weak driving: without coupling (blue); $v_x = 0.1, v_z = 0$ (red); $v_x = 0, v_z = 0.1$ (green). t-DMRG result (above) and its spectrum (below).

with $Q = 0$ and $Q = 1$ as the Rabi oscillations under QTN are a mixture of the two situations. The dominance of either case depends on the occupation rate of the impurity level. The influence of the QTN can be decreased if $\frac{v_z}{\Omega} \ll 1$ such that $\tilde{\Omega}' \approx \Omega'$ and $\tilde{P}_{\uparrow, max} \approx 1$. Thus it can be inferred, that reliable π -pulses can be performed under longitudinal QTN if the driving field is very strong $\Omega \gg v_z$. In particular for $\frac{v_z}{\Omega} \ll 1$ the maximum achievable probability $P_{\uparrow, max}$ can be estimated to

$$P_{\uparrow, max} = 1 - \left(\frac{v_z}{\Omega}\right)^2. \quad (3.16)$$

In contrast to that a v_x coupled QTN leads to damped Rabi oscillations. These damped oscillations can be roughly described with Γ_{\uparrow} and Γ_{\downarrow} by numerical evaluation of Eq.2.15 if the driving field term is added to H_0 . Under this transverse noise, pulses can operate properly if the Rabi cycle is short compared to the damping $\Omega \gg v_x$.

It can be concluded that a longitudinal noise changes the generalized Rabi frequency and resonance frequency which strongly reduces the Rabi amplitude, whereas the transverse coupled QTN causes damping which still allows relatively high Rabi amplitudes. Thus for dynamical decoupling it is very important to use strong and resonant pulses to get an effective noise cancelling.

3.5 Simulations of Spin Echo and Bang-Bang with Ideal π -Pulses

The t-DMRG simulation of pulses and pulse protocols together with QTN has various difficulties in choosing the right parameters and coupling strengths as described previously. Hence to obtain a result which can be used as a reference for later simulations, in the following part we do not use the term $\Omega \cos(\omega_d t) \sigma_x$ in the Hamiltonian. Instead π -pulses are implemented artificially by directly applying an operator $U = e^{i\frac{\pi}{2}\sigma_x}$ on the qubit state at a certain time τ . This performs an ideal infinitely strong and short π -pulse with the benefit that the pulse itself is not influenced by the QTN and only the time evolution of the pulse protocol can be observed. As in the following calculations the coherence of the qubit is the main observable, the qubit is initially prepared in an eigenstate of σ_x and v_z coupled to the QTN.

The first test case was the simulation of the spin echo protocol applied on a qubit coupled to QTN which was already done in Ref.[1]. This was performed by measuring the visibility $|D_{echo}(t)|$ where previously a π -pulse was applied at time $\tau = \frac{t}{2}$. The resulting spin echo signal is plotted in Fig.3.7 and it is very similar to the one presented in Ref.[1] Fig.5d which indicates that the t-DMRG implementation works properly. It can be seen that the decoherence of the qubit under the spin echo protocol is slower than without the pulses, however for longer times $\gamma t > 2.5$ the protocol has no positive effect.

In order to understand why the spin echo protocol does not work properly a simulation with iterated pulses with a spacing of t_{pulse} was done.

In Fig.3.8 it is clearly visible that after applying a π -pulse at time τ the qubit recovers

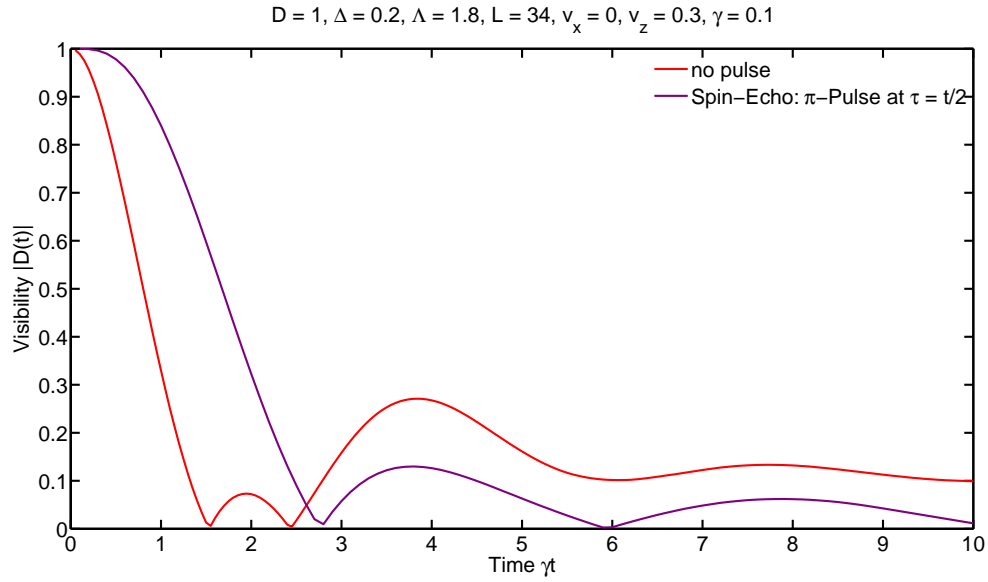


Figure 3.7: Spin-Echo: The purple curve shows visibility for times t when π -pulses were applied at $\tau = \frac{t}{2}$. The red curve shows the free decoherence. z-averaging was used.

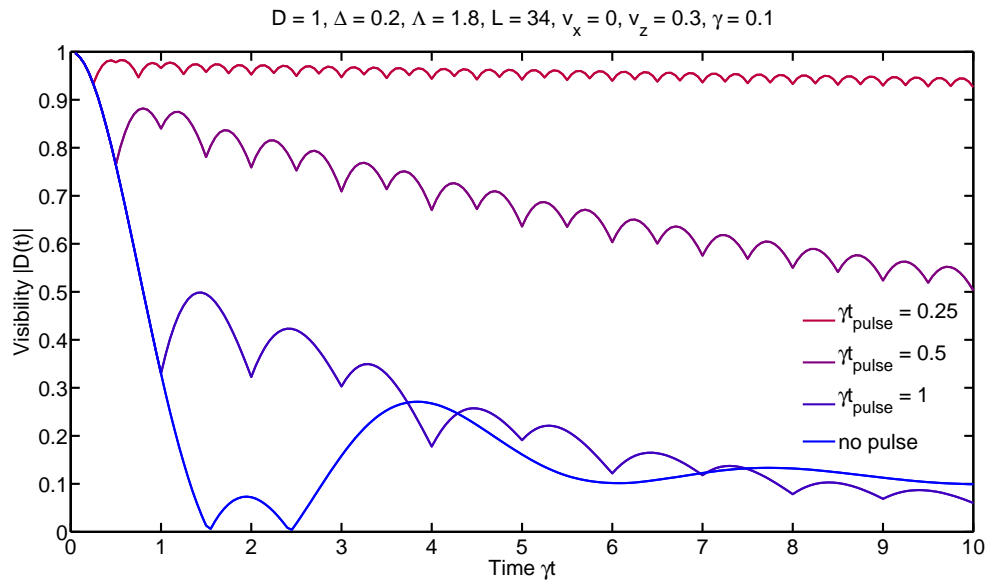


Figure 3.8: Bang-Bang protocol on a qubit prepared in σ_x eigenstate with QTN. π -pulses were applied after each interval of length γt_{pulse} . z-averaging was used.

a part of its coherence already at times $< 2\tau$. Subsequently it loses its coherence again leading to a decreased effect of the spin echo protocol. However this plot shows a much more interesting effect which is called bang-bang refocusing [15]. The iterated application of the pulses averages out the influence of the QTN leading to an almost only linearly decrease in coherence. Furthermore smaller intervals t_{pulse} between the bang-bang pulses improve the decoupling from the noise which is a result also found in the paper Ref.[15]. The improvement by the protocol mainly depends on the ratio $\frac{\tau_{bb}}{\tau_{noise}}$ of the time interval τ_{bb} between two bang-bang pulses and the mean separation τ_{noise} between two flips in the telegraph noise.

Chapter 4

Conclusion and Outlook

In this thesis the interaction between a qubit, a quantum telegraph noise (QTN) and an external periodical driving field was studied analytically, by deriving a quantum master equation for the qubit-QTN interaction and by presenting the Rabi problem and the Bloch-Siegert shift for the interaction between qubit and driving field. As this was only valid for the weak coupling regimes, t-DMRG simulations of the compound system were made to derive conditions under which π -pulses can be performed with good precision.

We started in Ch.2 with the description of the quantum telegraph noise model and found by calculating the bath correlation function that the quantum master equation in the Born-Markov approximation is valid for the case of $\gamma > \Delta$. This holds for high charge fluctuations on the impurity leading to a spectral broadening of $\frac{\gamma}{2}$ of its energy level which should be larger than the energy level spacing Δ of the qubit. Furthermore this can be brought to Lindblad form if the relaxation rate Γ of the qubit fulfills $\gamma > \Gamma > \Delta$. However as this analytical solution can not be applied to the case of $\frac{v}{\gamma} \geq 1$, where the QTN exhibits its non-Gaussian behavior, t-DMRG was used for all QTN calculations.

In Ch.3 Rabi oscillations were presented focusing on the Bloch-Siegert shift of the resonance frequency which occurs for strong driving amplitudes $\frac{\Omega}{\Delta} \geq 0.1$. As this effect also leads to a shift of the generalized Rabi frequency Ω' which determines the duration of a π -pulse by $\pi = \Omega't$, we presented an accurate method for measuring the Bloch-Siegert shift. Afterwards we have shown in Ch.3.4 that reliable π -pulses need to be very strong $\Omega \gg v$ compared to the coupling strength of the noise.

Finally simulations with ideal π -pulses in Ch.3.5 exhibited that the bang-bang protocol is very effective in preserving the coherence of a qubit whereas the spin echo protocol only marginally improved coherence time.

Further study could be conducted in the simulation of several pulse protocols, realized with the periodical driving field, for weak and strong coupling strengths to the QTN. Thereby the most suitable dynamical decoupling method for QTN can be found and the limits of protocol efficiency can be examined. An interesting extension of the model would be to investigate the coupling to more fluctuators and the influence on the coherence for different combinations of transverse and longitudinal coupling to a qubit. Another related topic is the effect of QTN on the Landau-Zener interference which can be simulated using an almost

similar Hamiltonian. This is very interesting as Landau-Zener interference could be used to measure decoherence rate of a qubit as proposed in Ref.[27].

Appendix A

Derivations

A.1 Master Equation

A.1.1 Projection Operator Method

The full derivation can be seen in Ref.[6, Ch.9.1] or Ref.[4, Ch.4]

We define the Liouville super operator L acting on the density matrix

$$\frac{d}{dt}\rho(t) = -i[H(t), \rho(t)] = L(t)\rho(t), \quad (\text{A.1})$$

and a set of orthogonal projection operators:

$$\begin{aligned} \mathcal{P}\rho &= \text{tr}_B(\rho) \otimes \rho_B = \rho_S \otimes \rho_B, \\ \mathcal{Q}\rho &= (\mathbb{1} - \mathcal{P})\rho, \\ (\mathcal{P} + \mathcal{Q}) &= \mathbb{1}. \end{aligned} \quad (\text{A.2})$$

For a Hamiltonian

$$H(t) = H_0 + \alpha H_I(t), \quad (\text{A.3})$$

we start from the Liouville super operator in the interaction picture \mathcal{L} :

$$\frac{d}{dt}\tilde{\rho}(t) = -i\alpha[\tilde{H}_I(t), \tilde{\rho}(t)] = \alpha\mathcal{L}(t)\tilde{\rho}(t). \quad (\text{A.4})$$

After inserting ones of projection operators

$$\frac{d}{dt}\tilde{\rho}(t) = \frac{d}{dt}(\mathcal{P} + \mathcal{Q})\tilde{\rho}(t) = \alpha\mathcal{L}(t)(\mathcal{P} + \mathcal{Q})\tilde{\rho}(t), \quad (\text{A.5})$$

we obtain two coupled differential equations

$$\frac{d}{dt}\mathcal{P}\tilde{\rho}(t) = \alpha\mathcal{P}\mathcal{L}\mathcal{P}\tilde{\rho} + \alpha\mathcal{P}\mathcal{L}\mathcal{Q}\tilde{\rho}, \quad (\text{A.6})$$

$$\frac{d}{dt}\mathcal{Q}\tilde{\rho}(t) = \underbrace{\alpha\mathcal{Q}\mathcal{L}\mathcal{P}\tilde{\rho}}_{\text{inhomogeneous}} + \underbrace{\alpha\mathcal{Q}\mathcal{L}\mathcal{Q}\tilde{\rho}}_{\text{homogeneous}}. \quad (\text{A.7})$$

First we solve homogeneous

$$\frac{d}{dt}\mathcal{Q}\tilde{\rho}(t) = \alpha\mathcal{Q}\mathcal{L}\mathcal{Q}\tilde{\rho} \rightarrow \mathcal{U}(t, t_0) = G(t, t_0) = \mathcal{T}e^{\alpha\int_{t_0}^t \mathcal{Q}\mathcal{L}(s)ds}, \quad (\text{A.8})$$

and inhomogeneous part

$$\Rightarrow \mathcal{Q}\tilde{\rho}(t) = G(t, t_0)\mathcal{Q}\tilde{\rho}(t_0) + \alpha\int_{t_0}^t ds G(t, s)\mathcal{Q}\mathcal{L}(s)\mathcal{P}\tilde{\rho}(s), \quad (\text{A.9})$$

of the differential equation in \mathcal{Q} and put the solution into Eq.A.6

$$\frac{d}{dt}\mathcal{P}\tilde{\rho}(t) = \alpha\mathcal{P}\mathcal{L}\mathcal{P}\tilde{\rho} + \alpha\mathcal{P}\mathcal{L}(t)G(t, t_0)\mathcal{Q}\tilde{\rho}(t_0) + \alpha^2\int_{t_0}^t ds\mathcal{P}\mathcal{L}(t)G(t, s)\mathcal{Q}\mathcal{L}(s)\mathcal{P}\tilde{\rho}(s). \quad (\text{A.10})$$

With pure initial states in system and bath $\rho(t_0) = \rho_S(t_0) \otimes \rho_B(t_0)$ and for a vanishing thermal expectation value $\langle H_I(t) \rangle_{\rho_B} = 0$ we get

$$\begin{aligned} \Rightarrow \mathcal{Q}\rho(t_0) &= 0, \\ \mathcal{P}\mathcal{L}\mathcal{P}\tilde{\rho}(t) &= 0, \end{aligned} \quad (\text{A.11})$$

reducing Eq.A.10 to

$$\frac{d}{dt}\mathcal{P}\tilde{\rho}(t) = \int_{t_0}^t ds \underbrace{\alpha^2\mathcal{P}\mathcal{L}(t)G(t, s)\mathcal{Q}\mathcal{L}(s)}_{\mathcal{K}(t,s)}\mathcal{P}\tilde{\rho}(s). \quad (\text{A.12})$$

For the weak coupling limit we expand Kernel $\mathcal{K}(t, s)$ to lowest order in α

$$\begin{aligned} G(t, s) &= \mathcal{T}e^{\alpha\int_{t_0}^t \mathcal{Q}\mathcal{L}(s)ds} \approx \mathbb{1} + \mathcal{O}(\alpha), \\ \Rightarrow \mathcal{K}(t, s) &\approx \alpha^2\mathcal{P}\mathcal{L}(t)\mathcal{Q}\mathcal{L}(s). \end{aligned} \quad (\text{A.13})$$

Thus

$$\begin{aligned} \frac{d}{dt}\mathcal{P}\tilde{\rho}(t) &= \int_{t_0}^t ds \alpha^2\mathcal{P}\mathcal{L}(t)\mathcal{Q}\mathcal{L}(s)\mathcal{P}\tilde{\rho}(s), \\ &\text{with } \mathcal{Q} = (\mathbb{1} - \mathcal{P}); \mathcal{P}\mathcal{L}(t)\mathcal{P} = 0, \\ \frac{d}{dt}\mathcal{P}\tilde{\rho}(t) &= \int_{t_0}^t ds \alpha^2\mathcal{P}\mathcal{L}(t)\mathcal{L}(s)\mathcal{P}\tilde{\rho}(s) \\ &= (-i)^2\alpha^2\int_{t_0}^t ds \mathcal{P} \left[\tilde{H}_I(t), \left[\tilde{H}_I(s), \tilde{\rho}_S(s) \otimes \rho_B \right] \right] \otimes \rho_B, \end{aligned} \quad (\text{A.14})$$

where the Born approximation was made in the last step. This assumes that the coupling between the bath and the qubit system is weak such that the influence of the open system on the bath is small. Therefore the state of the whole system can be expressed as $\tilde{\rho}(t) \approx$

$\tilde{\rho}_S(t) \otimes \rho_B$.

Finally we can apply \mathcal{P}

$$\frac{d}{dt}\tilde{\rho}_S(t) = -\alpha^2 \int_{t_0}^t ds \operatorname{tr}_B \left[\tilde{H}_I(t), \left[\tilde{H}_I(s), \tilde{\rho}_S(s) \otimes \rho_B \right] \right]. \quad (\text{A.15})$$

The Markov approximation assumes bath excitations to be decaying very fast which means that the whole system has no memory and does only depend on the present state $\tilde{\rho}_S(t)$ [6, p 127]. Therefore $\tilde{\rho}_S(s)$ can be replaced with $\tilde{\rho}_S(t)$ which makes the master equation local in time. Additionally a substitution $s \rightarrow t - s$ will be made and the upper limit of the integral will be extended to infinity, as the bath correlation function is considered to be fast decaying. Thus we obtain the quantum master equation in the Born-Markov approximation

$$\frac{d}{dt}\tilde{\rho}_S(t) = -\alpha^2 \int_0^\infty ds \operatorname{tr}_B \left[\tilde{H}_I(t), \left[\tilde{H}_I(t-s), \tilde{\rho}_S(t) \otimes \rho_B \right] \right]. \quad (\text{A.16})$$

A.1.2 Interaction Picture Hamiltonian

An arbitrary interaction Hamiltonian

$$H_I = \sum_{\alpha} A_{\alpha} \otimes B_{\alpha}, \quad (\text{A.17})$$

can be decomposed into eigenoperators $\Pi(\epsilon_i)$ of H_S which are the projectors into the eigenspaces of energies ϵ_i to simplify the calculation of \tilde{H}_I

$$\Pi(\epsilon_i) H_S = \epsilon_i. \quad (\text{A.18})$$

For a basis $|i\rangle$ diagonalizing H_S these are simply given by

$$\Pi(\epsilon_i) = |i\rangle \langle i|. \quad (\text{A.19})$$

The decomposition is defined as

$$\begin{aligned} A_{\alpha}(\omega) &= \sum_{\epsilon' - \epsilon = \omega} \Pi(\epsilon) A_{\alpha} \Pi(\epsilon'), \\ A_{\alpha} &= \sum_{\omega} A_{\alpha}(\omega), \\ A_{\alpha}(-\omega) &= A_{\alpha}^{\dagger}(\omega). \end{aligned} \quad (\text{A.20})$$

With the properties

$$\begin{aligned} [H_S, A_{\alpha}(\omega)] &= -\omega A_{\alpha}(\omega), \\ \Rightarrow U_0^{\dagger}(t) A_{\alpha}(\omega) U_0(t) &= e^{-i\omega t} A_{\alpha}(\omega) = \widetilde{A_{\alpha}(\omega)}(t), \end{aligned} \quad (\text{A.21})$$

the interaction picture Hamiltonian is

$$\begin{aligned}\tilde{H}_I(t) &= U_0^\dagger(t) \left(\sum_{\alpha,\omega} A_\alpha(\omega) \otimes B_\alpha \right) U_0(t) \\ &= \sum_{\alpha,\omega} e^{-i\omega t} A_\alpha(\omega) \otimes \tilde{B}_\alpha(t),\end{aligned}\tag{A.22}$$

which can be put into the master equation Eq.A.16

$$\begin{aligned}\frac{d}{dt} \tilde{\rho}_S(t) &= \sum_{\omega,\omega'} \sum_{\alpha,\beta} e^{i(\omega' - \omega)t} \Gamma_{\alpha\beta}(\omega) \left(A_\beta(\omega) \tilde{\rho}_S(t) A_\alpha^\dagger(\omega') - A_\alpha^\dagger(\omega') A_\beta(\omega) \tilde{\rho}_S(t) \right) + h.c., \\ \text{and } \Gamma_{\alpha\beta}(\omega) &= \int_0^\infty ds e^{i\omega s} \langle \tilde{B}_\alpha^\dagger(t) \tilde{B}_\beta(t-s) \rangle_{\rho_B}.\end{aligned}\tag{A.23}$$

Here $\Gamma_{\alpha\beta}(\omega)$ are the one-sided Fourier transforms of the bath correlation functions $\langle \tilde{B}_\alpha^\dagger(t) \tilde{B}_\beta(t-s) \rangle_{\rho_B}$. For the next step, the secular approximation, three important time scales have to be considered [6, p 130]. In accordance to the Markov approximation, the reservoir correlation functions $\langle \tilde{B}_\alpha^\dagger(s) \tilde{B}_\beta(0) \rangle_{\rho_B}$ decay fast over a time τ_B , if it is infinitely large and has a continuum of frequencies. This also means that relaxation time τ_R of the open system shall be large compared to τ_B . Above these the time scale of the intrinsic evolution of the open system τ_S , typically defined by $\frac{1}{|\omega' - \omega|}$ the inverse of the frequencies occurring, is large compared to τ_R and τ_B . This leads to the assumption that terms where $\omega' \neq \omega$ in Eq.A.23 are fast oscillating over τ_R and can be therefore neglected. With a decomposition of $\Gamma_{\alpha\beta}(\omega)$

$$\begin{aligned}\Gamma_{\alpha\beta}(\omega) &= \frac{1}{2} \gamma_{\alpha\beta}(\omega) + i S_{\alpha\beta}(\omega), \\ \gamma_{\alpha\beta}(\omega) &= \int_{-\infty}^\infty ds e^{i\omega s} \langle \tilde{B}_\alpha^\dagger(s) \tilde{B}_\beta(0) \rangle_{\rho_B}, \\ S_{\alpha\beta}(\omega) &= \frac{1}{2i} (\Gamma_{\alpha\beta}(\omega) - \Gamma_{\beta\alpha}^*(\omega)),\end{aligned}\tag{A.24}$$

and the definition of the Lamb shift Hamiltonian H_{LS}

$$H_{LS} = \sum_{\omega} \sum_{\alpha,\beta} S_{\alpha\beta}(\omega) A_\alpha^\dagger(\omega) A_\beta(\omega),\tag{A.25}$$

the master equation in the interaction picture under the assumption mentioned can be written as

$$\begin{aligned}\frac{d}{dt} \tilde{\rho}_S(t) &= -i [H_{LS}, \tilde{\rho}_S(t)] + \mathcal{D}(\tilde{\rho}_S(t)), \\ \mathcal{D}(\tilde{\rho}_S(t)) &= \sum_{\omega} \sum_{\alpha,\beta} \gamma_{\alpha\beta}(\omega) \left(A_\beta(\omega) \tilde{\rho}_S(t) A_\alpha^\dagger(\omega) - \frac{1}{2} \{ A_\alpha^\dagger(\omega) A_\beta(\omega), \tilde{\rho}_S(t) \} \right).\end{aligned}\tag{A.26}$$

The last term \mathcal{D} is also called the dissipator. As $A_\alpha(\omega)$ can be easily calculated for a given Hamiltonian, the only difficult expression is $\Gamma_{\alpha\beta}(\omega)$ which will be investigated in the following Chapter.

A.1.3 Bath Correlation Functions

In this section the Fourier transform of the bath correlation function according to our problem shall be calculated. The Hamiltonian we consider is normal ordered : $n := n - \langle n \rangle_{\rho_B}$ which leads to vanishing thermal expectation values of normal ordered operators. We start from

$$\tilde{B}(t) = \tilde{d}^\dagger(t)\tilde{d}(t), \quad (\text{A.27})$$

$$\Gamma(\omega) = \int_0^\infty ds e^{i\omega s} \langle \tilde{B}^\dagger(t)\tilde{B}(t-s) \rangle_{\rho_B} \quad (\text{A.28})$$

Using Wick's theorem the 4-point correlation function can be expressed by 2-point correlation functions

$$\langle \tilde{B}^\dagger(t)\tilde{B}(t-s) \rangle_{\rho_B} = \langle \tilde{B}^\dagger(s)\tilde{B}(0) \rangle_{\rho_B} = \langle \tilde{d}^\dagger(s)\tilde{d}(s)\tilde{d}^\dagger(0)\tilde{d}(0) \rangle_{\rho_B} \quad (\text{A.29})$$

$$= \underbrace{\tilde{d}^\dagger(s)\tilde{d}(s)}_{\langle \tilde{d}^\dagger(s)\tilde{d}(s) \rangle_{\rho_B}} \underbrace{\tilde{d}^\dagger(0)\tilde{d}(0)}_{\langle \tilde{d}^\dagger(0)\tilde{d}(0) \rangle_{\rho_B}} = \langle \tilde{d}^\dagger(s)\tilde{d}(0) \rangle_{\rho_B} \langle \tilde{d}(s)\tilde{d}^\dagger(0) \rangle_{\rho_B} \quad (\text{A.30})$$

From here we need certain relations on Green's functions

$$iG_{dd^\dagger}^>(t) = \langle \tilde{d}(t)\tilde{d}^\dagger(0) \rangle_{\rho_B}, \quad (\text{A.31})$$

$$iG_{dd^\dagger}^<(t) = -\langle \tilde{d}^\dagger(0)\tilde{d}(t) \rangle_{\rho_B}, \quad (\text{A.32})$$

$$G_{dd^\dagger}^>(\omega) = \frac{G_{dd^\dagger}^R(\omega) - G_{dd^\dagger}^A(\omega)}{e^{-\beta\omega} + 1}, \quad (\text{A.33})$$

$$G_{dd^\dagger}^<(\omega) = -\frac{G_{dd^\dagger}^R(\omega) - G_{dd^\dagger}^A(\omega)}{e^{\beta\omega} + 1}, \quad (\text{A.34})$$

$$G_{dd^\dagger}^R(\omega) = \frac{1}{\omega - \epsilon_d + i\frac{\gamma}{2}}, \quad (\text{A.35})$$

$$G_{dd^\dagger}^A(\omega) = \frac{1}{\omega - \epsilon_d - i\frac{\gamma}{2}}, \quad (\text{A.36})$$

$$\gamma = 2\pi \sum_k \|t_k\|^2 \delta(\epsilon_k - \epsilon_d). \quad (\text{A.37})$$

The relations for $G^R(\omega)$, $G^A(\omega)$ can be derived from equation of motion theory in imaginary time resulting in the Matsubara Green's function. This can be analytically continued to the retarded and advanced Green's functions. γ is the FWHM of the spectral broadening of the impurity level and corresponds to the parameter of the t-DMRG implementation. As it will be shown, γ also relates to the decay time of the bath correlation function $\tau_B = \frac{1}{\gamma}$, which is important for the Born-Markov approximation.

With these relations the expectation values can be identified

$$\langle \tilde{d}^\dagger(s)\tilde{d}(0) \rangle_{\rho_B} \langle \tilde{d}(s)\tilde{d}^\dagger(0) \rangle_{\rho_B} = G_{dd^\dagger}^<(-s)G_{dd^\dagger}^>(s), \quad (\text{A.38})$$

and the lesser and greater Green's functions can be calculated. We show the calculation in more detail for $G^>(t)$ starting from the explicit form of Eq.A.33

$$G_{dd^\dagger}^>(t) = \int_{-\infty}^{\infty} \frac{d\omega}{2\pi} e^{-i\omega t} \frac{1}{e^{-\beta\omega} + 1} \left(\frac{1}{\omega - \epsilon_d + i\frac{\gamma}{2}} - \frac{1}{\omega - \epsilon_d - i\frac{\gamma}{2}} \right). \quad (\text{A.39})$$

We perform the Fourier transformation using the residue theorem. As the function $G_{dd^\dagger}^>(s)$ is needed for times $s > 0$, the contour chosen must be closed over the lower half of the complex plane with $\Im(\omega) < 0$ to ensure the convergence of $e^{-i\omega t}$. Therefore we need to consider the poles of the first term at $\omega_n = -i\frac{\pi}{\beta}(2n+1)$ and of $G_{dd^\dagger}^R(\omega)$ at $\omega = \epsilon_d - i\frac{\gamma}{2}$. For the residue of the Fermi-Dirac distribution we have for $n \in \mathbb{Z}$

$$\text{Res} \left(\frac{1}{e^{\pm\beta\omega} + 1}, i\frac{\pi}{\beta}(2n+1) \right) = \mp \frac{1}{\beta}. \quad (\text{A.40})$$

Together with the series expansion of the Fermi-Dirac distribution

$$\frac{1}{e^{\pm\beta\omega} + 1} = \frac{1}{2} \mp \frac{1}{\beta} \sum_{n=-\infty}^{\infty} \frac{1}{\omega - i\frac{\pi}{\beta}(2n+1)}, \quad (\text{A.41})$$

the integral can be evaluated

$$\begin{aligned} iG_{dd^\dagger}^>(t) &= \frac{i}{4\pi} \int_{-\infty}^{\infty} d\omega e^{-i\omega t} \left(\frac{1}{\omega - \epsilon_d + i\frac{\gamma}{2}} - \frac{1}{\omega - \epsilon_d - i\frac{\gamma}{2}} \right) + \\ &+ \frac{i}{2\pi\beta} \sum_{n=-\infty}^{\infty} \int_{-\infty}^{\infty} d\omega \frac{e^{-i\omega t}}{\omega - i\frac{\pi}{\beta}(2n+1)} \left(\frac{1}{\omega - \epsilon_d + i\frac{\gamma}{2}} - \frac{1}{\omega - \epsilon_d - i\frac{\gamma}{2}} \right) \\ &\stackrel{t>0}{=} \frac{1}{2} e^{-i(\epsilon_d - i\frac{\gamma}{2})t} + \frac{1}{\beta} \sum_{n=-\infty}^{\infty} \frac{e^{-i(\epsilon_d - i\frac{\gamma}{2})t}}{\epsilon_d - i\frac{\gamma}{2} - i\frac{\pi}{\beta}(2n+1)} \\ &+ \frac{1}{\beta} \sum_{n=0}^{\infty} e^{-\frac{\pi}{\beta}(2n+1)t} \left(\frac{1}{-i\frac{\pi}{\beta}(2n+1) - \epsilon_d + i\frac{\gamma}{2}} - \frac{1}{-i\frac{\pi}{\beta}(2n+1) - \epsilon_d - i\frac{\gamma}{2}} \right). \end{aligned} \quad (\text{A.42})$$

The second expression can be rewritten using the partial fraction expansion of the hyperbolic tangent

$$\tanh(z) = \sum_{n=0}^{\infty} \frac{2}{2z - i(2n+1)\pi} + \frac{2}{2z + i(2n+1)\pi}, \quad (\text{A.43})$$

$$\begin{aligned}
\sum_{n=-\infty}^{\infty} \frac{1}{\epsilon_d - i\frac{\gamma}{2} - i\frac{\pi}{\beta}(2n+1)} &= \sum_{n=0}^{\infty} \left(\frac{1}{\epsilon_d - i\frac{\gamma}{2} - i\frac{\pi}{\beta}(2n+1)} + \frac{1}{\epsilon_d - i\frac{\gamma}{2} + i\frac{\pi}{\beta}(2n+1)} \right) \\
&= \frac{\beta}{2} \sum_{n=0}^{\infty} \left(\frac{2}{\beta(\epsilon_d - i\frac{\gamma}{2}) - i(2n+1)\pi} + \frac{2}{\beta(\epsilon_d - i\frac{\gamma}{2}) + i(2n+1)\pi} \right) \\
&= \frac{\beta}{2} \tanh \left(\frac{\beta}{2} \left(\epsilon_d - i\frac{\gamma}{2} \right) \right).
\end{aligned} \tag{A.44}$$

Hence we get

$$iG_{dd^\dagger}^>(t) \stackrel{t \geq 0}{=} \frac{e^{-i(\epsilon_d - i\frac{\gamma}{2})t}}{2} \left(\tanh \left(\frac{\beta}{2} \left(\epsilon_d - i\frac{\gamma}{2} \right) \right) + 1 \right) + \frac{1}{\beta} \sum_{n=0}^{\infty} \frac{-i\gamma e^{-\frac{\pi}{\beta}(2n+1)t}}{\left(\epsilon_d + i\frac{\pi}{\beta}(2n+1) \right)^2 + \left(\frac{\gamma}{2} \right)^2}. \tag{A.45}$$

By analogy an expression for $G_{dd^\dagger}^<(t)$ can be found by closing the contour over the upper half plane as we need $t < 0$

$$iG_{dd^\dagger}^<(t) \stackrel{t \leq 0}{=} \frac{e^{-i(\epsilon_d + i\frac{\gamma}{2})t}}{2} \left(\tanh \left(\frac{\beta}{2} \left(\epsilon_d + i\frac{\gamma}{2} \right) \right) - 1 \right) - \frac{1}{\beta} \sum_{n=0}^{\infty} \frac{-i\gamma e^{\frac{\pi}{\beta}(2n+1)t}}{\left(\epsilon_d - i\frac{\pi}{\beta}(2n+1) \right)^2 + \left(\frac{\gamma}{2} \right)^2}. \tag{A.46}$$

Since these expressions are very long and complicated, the limit of low temperatures will be considered. For $\beta \rightarrow \infty$ the last term vanishes

$$iG_{dd^\dagger}^{\gtrless}(t) = \theta(\pm t) \frac{e^{-i(\epsilon_d \mp i\frac{\gamma}{2})t}}{2} \left(\tanh \left(\frac{\beta}{2} \left(\epsilon_d \mp i\frac{\gamma}{2} \right) \right) \pm 1 \right). \tag{A.47}$$

It can be seen that the bath correlation function decays with the time $\tau_B = \frac{1}{\gamma}$ as it has terms which are products of two Green's functions each decaying with rate $\frac{\gamma}{2}$.

From here it is possible to continue calculating Eq.A.28

$$\Gamma(\omega) = \int_0^\infty ds e^{i\omega s} \langle \tilde{B}^\dagger(t) \tilde{B}(t-s) \rangle_{\rho_B} = \int_0^\infty ds e^{i\omega s} G_{dd^\dagger}^>(s) G_{dd^\dagger}^<(-s) \tag{A.48}$$

$$= \frac{1-i\omega-\gamma}{4\omega^2+\gamma^2} \left(\tanh \left(\frac{\beta}{2} \left(\epsilon_d - i\frac{\gamma}{2} \right) \right) + 1 \right) \left(\tanh \left(\frac{\beta}{2} \left(\epsilon_d + i\frac{\gamma}{2} \right) \right) - 1 \right). \tag{A.49}$$

In order to get the relaxation and dephasing rates for the master equation and the Lamb shift we have to calculate

$$\gamma(\omega) = \Gamma(\omega) + \Gamma(\omega)^*, \tag{A.50}$$

$$S(\omega) = \frac{1}{2i} (\Gamma(\omega) - \Gamma(\omega)^*), \tag{A.51}$$

which can be done numerically and is shown in Fig.2.2 for different temperatures. It should be mentioned that $\gamma(\omega) \neq \gamma$.

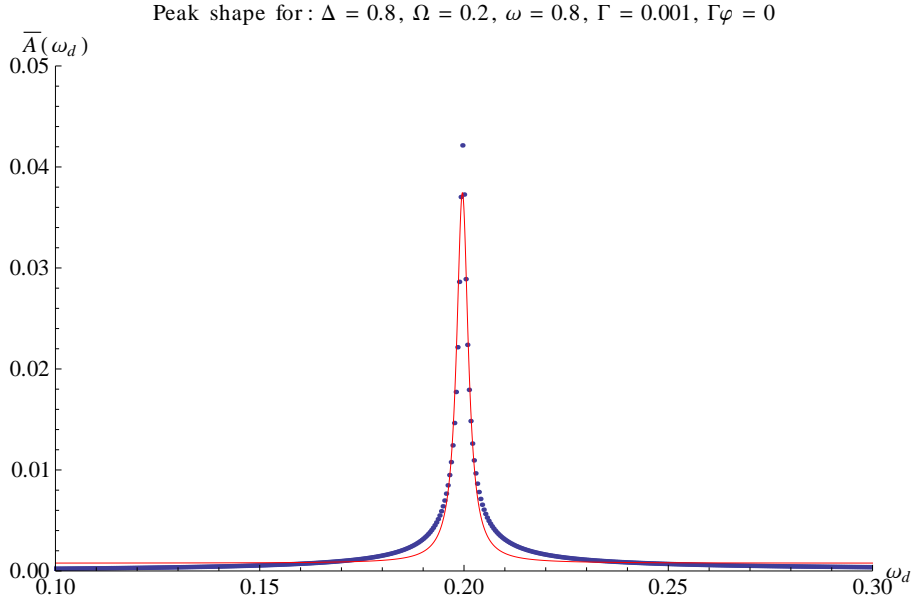


Figure A.1: Peak of Ω' after DFT from numerical results with very weak damping. Lorentzian fit (red) is not accurate enough for amplitude measurement.

A.2 Discrete Fourier Transformation

For the spectral evaluation of the Rabi peak in both methods, a Fourier transformation is needed. As data from the DMRG simulation as well as from calculations with Mathematica/MATLAB are only given as a finite number of discrete values, a discrete Fourier transformation must be applied. There are several normalization conventions in the literature, depending on the specific application. We use

$$H(\omega_k) = \frac{1}{N} \sum_{n=0}^{N-1} P_{\uparrow}(t_n) e^{2\pi i \frac{nk}{N}}, \quad (\text{A.52})$$

$$\bar{A}(\omega_k) = |2H(\omega_k)|,$$

where $N = T \cdot f_s$. This normalizes the peaks such that $H(\omega_k)$ equals to the half average amplitude of an oscillation with frequency $|\omega_k|$, as it contains only values for ω_k and not for $-\omega_k$. Thus the average amplitude is given by $\bar{A}(\omega_k)$, which will be used as the result of the DFT. With these definitions a full resonant Rabi oscillation without damping gives $\bar{A}(\Omega') = 0.5$ as the maximum amplitude equals to 0.5.

As only a discrete Fourier transformation is performed, the total time T should be as long as possible to get a high frequency resolution (small $\Delta\omega$) together with a small error in peak amplitudes. The sampling frequency f_s , determining the maximal resolvable frequency $\omega = \pi f_s$ according to the Nyquist-Shannon sampling theorem, should also be as large as possible. If we consider computation time, smaller values of both are better.

However smaller values have to be chosen cautiously, as a too small f_s results in artifacts due to cutting a not bandwidth limited signal. Thus $f_s \sim 2\omega_d + 2\Omega$ will be used as a good compromise, for higher order peaks being of a negligible strength. This choice still allows seeing the higher order peaks which produce the steps in Fig.3.1.

The peaks retrieved from the spectrum are of a very sharp Lorentzian type shape consisting only of a few points which makes it impossible to read off the desired values of amplitude and position precisely (see Fig.A.1). Therefore two ways of improving this measurement were used.

The first one takes advantage of a broadened peak when adding a damping to the qubit which then enables to fit a modified Lorentzian curve and read off the values as fit parameters. While the data generated by DMRG already contain the damping from the QTN and can be used directly, the simulation in Mathematica needs a modified differential equation. Therefore the equation of motion for the density matrix with the damping coefficient Γ is

$$\frac{d}{dt}\rho = -i[H, \rho] + \Gamma (L[\sigma^+]\rho + L[\sigma^-]\rho), \quad (\text{A.53})$$

with the Hamiltonian H given by Eq.3.2. This differential equation can be numerically solved to receive the data. After applying the DFT a modified Lorentzian function of the form

$$F(x) = C \frac{1}{\pi} \frac{s}{s^2 + (x - m)^2} + a, \quad (\text{A.54})$$

is fitted to the peak yielding the desired results:

$$\begin{aligned} \bar{A}(\Omega') &= \frac{C}{\pi s} + a, \\ \Omega' &= m. \end{aligned} \quad (\text{A.55})$$

The second method is called zero padding using a rectangular window which on the one hand adds artifacts, known as the spectral leakage, to the Fourier transformed data but on the other hand enhances peak resolution. Hence the peaks cannot be fitted anymore but read off directly instead, which is quite accurate for measuring the peak positions. Before applying the DFT, the dataset will be enlarged to a size M by filling it with zeros which costs much less computing time than increasing N and actually calculating the data. As it can be seen in Fig.A.2 this method interpolates the standard DFT. But as this padding has also an effect similar to multiplying the data by a rectangular window function, the Fourier transform is now a convolution of the original DFT and a Sinc-function, which results in the spectral leakage. Because only the peak itself is to be measured this is not such an important problem, but it contributes errors to the amplitude measurement.

A similar effect can be achieved by rescaling the transformation without adding zeros to the dataset

$$H(\omega_k) = \frac{1}{N} \sum_{n=0}^{N-1} P_{\uparrow}(t_n) e^{2\pi i \frac{nk}{N} * \frac{\omega_{max}}{2\pi f_s}}. \quad (\text{A.56})$$

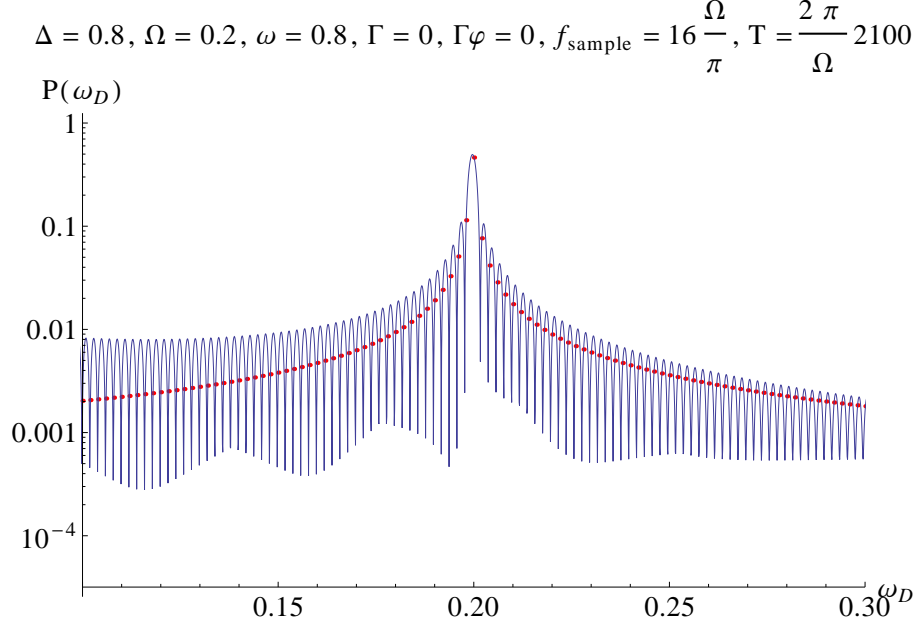


Figure A.2: Peak shape with standard DFT (red) and with zero padding by a factor of $\frac{M}{N} = 21$ using a rectangular window (blue). Spectral leakage is visible as oscillating errors next to the peak.

This is equivalent to the DFT calculation of only the first N frequencies of a dataset which was enlarged by a factor of $\frac{M}{N} = \frac{2\pi f_s}{\omega_{max}}$ with zero padding.

The data can also be multiplied with a flat-top window before performing the zero padding and the DFT. The window is defined according to the MATLAB definition

$$\begin{aligned}
 w(n) &= a_0 + a_1 \cos\left(2\pi \frac{n}{N}\right) + a_2 \cos\left(4\pi \frac{n}{N}\right) + a_3 \cos\left(6\pi \frac{n}{N}\right) + a_4 \cos\left(8\pi \frac{n}{N}\right), \\
 a_0 &= 0.21557895, \\
 a_1 &= -0.41663158, \\
 a_2 &= 0.277263158, \\
 a_3 &= -0.083578947, \\
 a_4 &= 0.006947368.
 \end{aligned} \tag{A.57}$$

It has the advantage of a better amplitude measurement but with a higher error in peak position. Using the second method a Lorentzian fit is not sensible anymore, because of the sinc-type peak shape and the spectral leakage, but the position and amplitude of the Rabi peak can now easily be extracted by searching for the maximum without fitting.

A.3 Solution of the Rabi Problem

The Schrödinger equation for the driven two-level system will now be solved explicitly under the two mentioned approximations in order to derive the relations given in Ch.3.2. For convenience the convention $\hbar = 1$ will be used throughout all calculations. The Schrödinger equation is given by

$$i \frac{d}{dt} |\Psi(t)\rangle = (H_0 + H_1(t)) |\Psi(t)\rangle = \left(\frac{\Delta}{2} \sigma_z + \Omega \cos(\omega_d t) \sigma_x \right) |\Psi(t)\rangle. \quad (\text{A.58})$$

First the homogenous part H_0 will be solved with the ansatz

$$|\Psi(t)\rangle = C_1(t) e^{-i\frac{\Delta}{2}t} |\uparrow\rangle + C_2(t) e^{i\frac{\Delta}{2}t} |\downarrow\rangle, \quad (\text{A.59})$$

where already the variation of the constants $C_i(t)$ has been applied. The states $|\uparrow\rangle, |\downarrow\rangle$ are the eigenstates of the σ_z operator according to the eigenvalues $1, -1$. Putting this into Eq.A.58 yields a coupled differential equation in the interaction picture for the interaction term $H_1(t)$

$$\begin{aligned} i\dot{C}_1(t) &= \Omega \cos(\omega_d t) e^{i\Delta t} C_2(t), \\ i\dot{C}_2(t) &= \Omega \cos(\omega_d t) e^{-i\Delta t} C_1(t). \end{aligned} \quad (\text{A.60})$$

With the relation $\cos(\omega t) = \frac{1}{2} (e^{i\omega t} + e^{-i\omega t})$ this gives

$$\begin{aligned} i\dot{C}_1(t) &= \frac{\Omega}{2} (e^{i(\Delta+\omega_d)t} + e^{i(\Delta-\omega_d)t}) C_2(t), \\ i\dot{C}_2(t) &= \frac{\Omega}{2} (e^{-i(\Delta+\omega_d)t} + e^{-i(\Delta-\omega_d)t}) C_1(t). \end{aligned} \quad (\text{A.61})$$

As this coupled differential equation is not easy to solve two different approximations will be made to get the wanted relations.

A.3.1 Rotating-Wave-Approximation

The reason for applying the Rotating-Wave-Approximation is that the result of interest is the overall transition behavior between up and down state of the qubit, which happens on a long time scale of order $\frac{2\pi}{\Omega}$ with $\Omega < \Delta$. Therefore terms with $e^{\pm i(\Delta+\omega_d)t}$ will be neglected in the RWA as they are rapidly oscillating in comparison to terms with $e^{\pm i(\Delta-\omega_d)t}$ especially for a nearly resonant driving $\omega_d \sim \Delta$. This simplifies the differential equations to

$$\begin{aligned} i\dot{C}_1(t) &= \frac{\Omega}{2} e^{i(\Delta-\omega_d)t} C_2(t), \\ i\dot{C}_2(t) &= \frac{\Omega}{2} e^{-i(\Delta-\omega_d)t} C_1(t), \end{aligned} \quad (\text{A.62})$$

which can be solved with the ansatz of $C_1(t) = Ae^{-i\lambda t}$. Putting this into both equations and eliminating \dot{C}_2 by taking the derivative of the first expression gives

$$i\dot{C}_2(t) = \frac{A\Omega}{2}e^{-i(\Delta-\omega_d+\lambda)t} = (\Delta - \omega_d + \lambda)\frac{2A\lambda}{\Omega}e^{-i(\Delta-\omega_d+\lambda)t}, \quad (\text{A.63})$$

$$\lambda_{\pm} = -\frac{\Delta - \omega_d}{2} \pm \frac{1}{2}\underbrace{\sqrt{(\Delta - \omega_d)^2 + \Omega^2}}_{\Omega'}. \quad (\text{A.64})$$

As a remark, for resonance $\omega_d = \Delta$: $\lambda_{\pm} = \pm\frac{\Omega}{2}$.

The solution in the interaction picture is as follows

$$\begin{aligned} C_1(t) &= Ae^{-i\lambda_+t} + Be^{-i\lambda_-t}, \\ C_2(t) &= \frac{2}{\Omega}e^{-i(\Delta-\omega_d)t} (A\lambda_+e^{-i\lambda_+t} + B\lambda_-e^{-i\lambda_-t}). \end{aligned} \quad (\text{A.65})$$

Together with the initial conditions $C_1(0) = 0, C_2(0) = 1$, meaning that the qubit is prepared in its ground state, this gives

$$\begin{aligned} C_1(t) &= i\frac{\Omega}{\Omega'} \sin\left(\frac{\Omega'}{2}t\right) e^{i\frac{\Delta-\omega_d}{2}t}, \\ C_2(t) &= \left(\cos\left(\frac{\Omega'}{2}t\right) + i\frac{\Delta - \omega_d}{\Omega'} \sin\left(\frac{\Omega'}{2}t\right)\right) e^{-i\frac{\Delta-\omega_d}{2}t}. \end{aligned} \quad (\text{A.66})$$

From these amplitudes the probabilities are calculated by $P_i(t) = |C_i(t)|^2$

$$\begin{aligned} P_{\uparrow}(t) &= \frac{\Omega^2}{\Omega'^2} \sin^2\left(\frac{\Omega'}{2}t\right), \\ P_{\downarrow}(t) &= 1 - \frac{\Omega^2}{\Omega'^2} \sin^2\left(\frac{\Omega'}{2}t\right). \end{aligned} \quad (\text{A.67})$$

A.3.2 Bloch-Siegert Shift

Starting from Eq.A.61 in this calculation the terms with $e^{\pm i(\Delta-\omega)t}$ will be neglected as we are now only interested in the contribution of the high oscillating field near resonance [31]. This simplifies the equations to

$$\begin{aligned} i\dot{C}_1(t) &= \frac{\Omega}{2}e^{i(\Delta+\omega_d)t}C_2(t), \\ i\dot{C}_2(t) &= \frac{\Omega}{2}e^{-i(\Delta+\omega_d)t}C_1(t), \end{aligned} \quad (\text{A.68})$$

which can be solved with an ansatz $C_1(t) = Ae^{-i\lambda t}$ yielding

$$\lambda_{\pm} = -\frac{\Delta + \omega_d}{2} \pm \frac{1}{2}\sqrt{(\Delta + \omega_d)^2 + \Omega^2}. \quad (\text{A.69})$$

This gives the solution in the interaction picture with arbitrary constants A, B

$$\begin{aligned} C_1(t) &= Ae^{-i\lambda_+t} + \frac{2\lambda_-}{\Omega}Be^{-i\lambda_-t}, \\ C_2(t) &= \frac{2\lambda_+}{\Omega}Ae^{i\lambda_-t} + Be^{i\lambda_+t}. \end{aligned} \tag{A.70}$$

After this step the assumption of $\Omega < \omega_d, \Delta$ will be made. This allows the approximations $\lambda_+ \simeq \frac{\Omega^2}{4(\Delta + \omega_d)}$, $\lambda_- \simeq -(\Delta + \omega_d)$ which can further simplify the solution by ignoring small amplitudes of order $\frac{\Omega}{\Delta} \ll 1$

$$\begin{aligned} C_1(t) &= Ae^{-i\lambda_+t}, \\ C_2(t) &= Be^{i\lambda_+t}. \end{aligned} \tag{A.71}$$

Back in the Schrödinger picture we get

$$\Psi(t) \simeq \begin{pmatrix} Ae^{-i(\frac{\Delta}{2} + \lambda_+)t} \\ Be^{i(\frac{\Delta}{2} + \lambda_+)t} \end{pmatrix}. \tag{A.72}$$

From this we can see that the energies of the upper and lower levels are shifted by λ_+ and the corrected energy spacing of the qubit due to the shift is

$$\Delta' = \Delta + 2\lambda_+ = -\omega_d + \sqrt{(\Delta + \omega_d)^2 + \Omega^2}. \tag{A.73}$$

So a resonant driving is now obtained via $\omega_d = \Delta'$, which gives the resonance condition according to the Bloch-Siegert shift for ω_{BS}

$$\begin{aligned} \omega_{BS} &= \frac{1}{2}\sqrt{(\Delta + \omega_{BS})^2 + \Omega^2}, \\ \omega_{BS} &= \Delta \left(\frac{1}{3} + \frac{2}{3}\sqrt{1 + \frac{3\Omega^2}{4\Delta^2}} \right) \\ &\stackrel{\Omega \leq \Delta}{\simeq} \Delta \left(1 + \frac{\Omega^2}{4\Delta^2} \right), \\ \Rightarrow \Delta\omega_{BS} &\simeq \frac{\Omega^2}{4\Delta}. \end{aligned} \tag{A.74}$$

The last expression is known as the Bloch-Siegert shift. The same result can be obtained by claiming the generalized Rabi frequency under the Bloch-Siegert shift Ω'_{BS} to be minimized at resonance.

A.4 Jaynes-Cummings-Hamiltonian

After describing the semi-classical Rabi dynamics in Ch.A.3, the fully quantum mechanical Jaynes-Cummings-model will be explained here. The first step is the replacement of the

classical driving with the quantized field in Eq.3.2. The following Hamiltonian is of a form commonly used in quantum optics

$$H = \frac{\hbar\omega_0}{2}\sigma_z + \hbar\omega_d \left(b^\dagger b + \frac{1}{2} \right) + \hbar g \hat{E} \sigma_x = H_{qubit} + H_{EM} + H_I. \quad (\text{A.75})$$

With symbols and conventions used in this thesis, the operator of a single mode electromagnetic field $\hat{E} = \sqrt{\frac{\hbar\omega_d}{\epsilon_0 V}} (b + b^\dagger)$ as well as $\sigma_x = \sigma^+ + \sigma^-$ this can be rewritten as

$$H = \frac{\Delta}{2}\sigma_z + \omega_d \left(b^\dagger b + \frac{1}{2} \right) + \frac{\Omega_0}{2} (\sigma^+ b + \sigma^- b^\dagger + \sigma^+ b^\dagger + \sigma^- b). \quad (\text{A.76})$$

With $H_0 = H_{qubit} + H_{EM}$ and Eq.A.21 the interaction picture Hamiltonian reads

$$\begin{aligned} \tilde{H}_I(t) &= U_0^\dagger(t) H_I(t) U_0(t) \\ &= \frac{\Omega_0}{2} (\sigma^+ b e^{i(\Delta-\omega_d)t} + \sigma^- b^\dagger e^{-i(\Delta-\omega_d)t} + \sigma^+ b^\dagger e^{i(\Delta+\omega_d)t} + \sigma^- b e^{-i(\Delta+\omega_d)t}). \end{aligned} \quad (\text{A.77})$$

Similar to the RWA in Ch.A.3.1 terms with $e^{\pm i(\Delta+\omega_d)t}$ will be neglected here as well yielding the Jaynes-Cummings-Hamiltonian

$$H_{JC} = \frac{\Delta}{2}\sigma_z + \omega_d \left(b^\dagger b + \frac{1}{2} \right) + \frac{\Omega_0}{2} (\sigma^+ b + \sigma^- b^\dagger), \quad (\text{A.78})$$

with Δ as the qubit energy level splitting and Ω_0 the vacuum Rabi frequency. b^\dagger and b are the creation and annihilation operators of a photon with field energy ω_d (here only one mode will be considered e.g. laser). We are interested in the time-evolution of the states $|g, n+1\rangle$, for the system in ground state and $n+1$ photons in field, and $|e, n\rangle$ corresponding to an excited system and n photons in the field

$$|\Psi_0\rangle = b_{g,n+1}(0) |g, n+1\rangle + b_{e,n}(0) |e, n\rangle. \quad (\text{A.79})$$

By solving the two coupled differential equations retrieved from the Schrödinger equation for this initial state, we get the quantized Rabi frequency Ω_n

$$\Omega_n = \Omega_0 \sqrt{n+1}, \quad (\text{A.80})$$

which depends on the number of photons in the field mode. For the initial state $|\Psi(0)\rangle = |g, n+1\rangle$ and resonance we obtain

$$|\Psi(t)\rangle = \cos\left(\frac{\Omega_n t}{2}\right) |g, n+1\rangle + i \frac{\Omega_0}{|\Omega_0|} \sin\left(\frac{\Omega_n t}{2}\right) |e, n\rangle. \quad (\text{A.81})$$

Thus the probabilities for ground and excited state are

$$P_g(t) = |\langle g | \Psi(t) \rangle|^2 = \cos^2\left(\frac{\Omega_n t}{2}\right), \quad (\text{A.82})$$

$$P_e(t) = |\langle e | \Psi(t) \rangle|^2 = \sin^2\left(\frac{\Omega_n t}{2}\right). \quad (\text{A.83})$$

The result is very close to the semiclassical solution. Considering Ω_n we can also see that for a field mode with many photons $n \gg 1$ the Rabi frequency loses its quantized character, which can basically be understood as the classical limit. This means that strong π -pulses which have high intensities $\langle I \rangle = \langle b^\dagger b \rangle = \langle N \rangle$ can be described by using the classical fields leading to the semiclassical description of Rabi dynamics Ch.A.3.

Bibliography

- [1] ABEL, B., AND MARQUARDT, F. Decoherence by quantum telegraph noise: A numerical evaluation. *Phys. Rev. B* 78 (Nov 2008), 201302.
- [2] ABEL, B. S. *Macroscopic superposition states and decoherence by quantum telegraph noise*. PhD thesis, LMU Munich, 03 2009.
- [3] ALLEN, L., AND EBERLY, J. *Optical Resonance and Two-Level Atoms*. Dover Books on Physics. Dover, 1987.
- [4] BAUER, M. Lindblad driving for nonequilibrium steady-state transport for noninteracting quantum impurity models, 07 2011. Bachelor thesis, LMU Munich.
- [5] BLOCH, F., AND SIEGERT, A. Magnetic resonance for nonrotating fields. *Phys. Rev.* 57 (Mar 1940), 522–527.
- [6] BREUER, H., AND PETRUCCIONE, F. *The Theory of Open Quantum Systems*. Oxford University Press, 2002.
- [7] BRUUS, H., AND FLENSBERG, K. *Many-body Quantum Theory In Condensed Matter Physics: An Introduction*. Oxford graduate texts in mathematics. Oxford University Press, 2004.
- [8] BULLA, R., COSTI, T. A., AND PRUSCHKE, T. Numerical renormalization group method for quantum impurity systems. *Rev. Mod. Phys.* 80 (Apr 2008), 395–450.
- [9] CARDOSO, G. C., PRADHAN, P., MORZINSKI, J., AND SHAHRIAR, M. S. *In situ* detection of the temporal and initial phase of the second harmonic of a microwave field via incoherent fluorescence. *Phys. Rev. A* 71 (Jun 2005), 063408.
- [10] CARR, H. Y., AND PURCELL, E. M. Effects of diffusion on free precession in nuclear magnetic resonance experiments. *Phys. Rev.* 94 (May 1954), 630–638.
- [11] EKERT, A., HAYDEN, P. M., AND INAMORI, H. Course 10: Basic concepts in quantum computation. In *Coherent Atomic Matter Waves* (2001), R. Kaiser, C. Westbrook, and F. David, Eds., p. 661.

-
- [12] GONZALEZ-TUDELA, A., DEL VALLE, E., CANCELLIERI, E., TEJEDOR, C., SANVITTO, D., AND LAUSSY, F. P. Effect of pure dephasing on the jaynes-cummings nonlinearities. *Opt. Express* 18, 7 (Mar 2010), 7002–7009.
- [13] GRISHIN, A., YURKEVICH, I. V., AND LERNER, I. V. Low-temperature decoherence of qubit coupled to background charges. *Phys. Rev. B* 72 (Aug 2005), 060509.
- [14] GUO, C., WEICHSELBAUM, A., KEHREIN, S., XIANG, T., AND VON DELFT, J. Density matrix renormalization group study of a quantum impurity model with landau-zener time-dependent hamiltonian. *Phys. Rev. B* 79 (Mar 2009), 115137.
- [15] GUTMANN, H., WILHELM, F. K., KAMINSKY, W. M., AND LLOYD, S. Bang–bang refocusing of a qubit exposed to telegraph noise. *Quantum Information Processing* 3 (2004), 247–272. 10.1007/s11128-004-2223-0.
- [16] HAHN, E. L. Spin echoes. *Phys. Rev.* 80 (Nov 1950), 580–594.
- [17] KHODJASTEH, K., AND LIDAR, D. A. Fault-tolerant quantum dynamical decoupling. *Phys. Rev. Lett.* 95 (Oct 2005), 180501.
- [18] LDS DACTRON. *Understanding FFT windows*.
- [19] MEIBOOM, S., AND GILL, D. Modified spin - echo method for measuring nuclear relaxation times. *Rev. Sci. Instrum.* 29, 8 (May 1958), 688–691.
- [20] NAKAMURA, Y. Quantum coherence in josephson-junction qubits, 2003.
- [21] NAKAMURA, Y., PASHKIN, Y. A., YAMAMOTO, T., AND TSAI, J. S. Charge echo in a cooper-pair box. *Phys. Rev. Lett.* 88 (Jan 2002), 047901.
- [22] OZAKI, T. Continued fraction representation of the fermi-dirac function for large-scale electronic structure calculations. *Phys. Rev. B* 75 (Jan 2007), 035123.
- [23] PAIK, H., SCHUSTER, D. I., BISHOP, L. S., KIRCHMAIR, G., CATELANI, G., SEARS, A. P., JOHNSON, B. R., REAGOR, M. J., FRUNZIO, L., GLAZMAN, L. I., GIRVIN, S. M., DEVORET, M. H., AND SCHOELKOPF, R. J. Observation of high coherence in josephson junction qubits measured in a three-dimensional circuit qed architecture. *Phys. Rev. Lett.* 107 (Dec 2011), 240501.
- [24] PRADHAN, P., CARDOSO, G. C., AND SHAHRIAR, M. S. Suppression of error in qubit rotations due to bloch–siebert oscillation via the use of off-resonant raman excitation. *J. Phys. B: At. Mol. Opt. Phys.* 42, 6 (Mar 2009), 065501.
- [25] RAMMER, J., AND SMITH, H. Quantum field-theoretical methods in transport theory of metals. *Rev. Mod. Phys.* 58 (Apr 1986), 323–359.
- [26] RIVAS, Á., AND HUELGA, S. F. Open quantum systems. an introduction. *ArXiv e-prints* (Apr. 2011).

- [27] RUDNER, M. S., SHYTOV, A. V., LEVITOV, L. S., BERNS, D. M., OLIVER, W. D., VALENZUELA, S. O., AND ORLANDO, T. P. Quantum phase tomography of a strongly driven qubit. *Phys. Rev. Lett.* *101* (Nov 2008), 190502.
- [28] SAKURAI, J., AND TUAN, S. *Modern Quantum Mechanics*. Addison-Wesley Publishing Company, 1994.
- [29] SCHOLLWÖCK, U. The density-matrix renormalization group in the age of matrix product states. *Annals of Physics* *326*, 1 (2011), 96–192.
- [30] SHAHRIAR, M. S., PRADHAN, P., AND MORZINSKI, J. Driver-phase-correlated fluctuations in the rotation of a strongly driven quantum bit. *Phys. Rev. A* *69* (Mar 2004), 032308.
- [31] SONODA, H. The bloch-siegert shift, Jun 2011.
- [32] UHRIG, G. S. Keeping a quantum bit alive by optimized π -pulse sequences. *Phys. Rev. Lett.* *98* (Mar 2007), 100504.
- [33] VAN DER SAR, T., WANG, Z. H., BLOK, M. S., BERNIEN, H., TAMINIAU, T. H., TOYLI, D. M., LIDAR, D. A., AWSCHALOM, D. D., HANSON, R., AND DOBROVITSKI, V. V. Decoherence-protected quantum gates for a hybrid solid-state spin register. *Nature* *484* (Apr 2012), 82.
- [34] VIOLA, L., KNILL, E., AND LLOYD, S. Dynamical decoupling of open quantum systems. *Phys. Rev. Lett.* *82* (Mar 1999), 2417–2421.
- [35] VIOLA, L., AND LLOYD, S. Dynamical suppression of decoherence in two-state quantum systems. *Phys. Rev. A* *58* (Oct 1998), 2733–2744.
- [36] VON DELFT, J., AND YEVTUSHENKO, O. Many-body physics. Lecture Notes, 2011.
- [37] XIAO, Z., HE, L., AND GE WANG, W. Efficiency of dynamical decoupling sequences in the presence of pulse errors. *Phys. Rev. A* *83* (Mar 2011), 032322.
- [38] ZRENNER, A., BEHAM, E., STUFLER, S., FINDEIS, F., BICHLER, M., AND ABSTREITER, G. Coherent properties of a two-level system based on a quantum-dot photodiode. *Nature* *418*, 6898 (2002), 612–614. 10.1038/nature00912.

Acknowledgements

I would like to thank my supervisor Prof. Jan von Delft for suggesting me this very interesting topic and for the inspiring discussions. Furthermore I want to thank Prof. Florian Marquardt for giving me good advice.

In particular I want to express my gratitude to Cheng Guo who supported me greatly whenever I needed help.

Finally I wish to thank the German National Academic Foundation (Studienstiftung) and the Max-Weber-Programm for financial and non-material support during the entire time of my studies.

Erklärung

Hiermit erkläre ich, dass ich die vorgelegte Arbeit selbstständig angefertigt und keine anderen als die angegebenen Quellen und Hilfsmittel verwendet habe.

München, den 20.07.2012

Schröder, Florian